Chem Soc Rev

Cite this: *Chem. Soc. Rev.*, 2012, **41**, 7228–7246

www.rsc.org/csr

CRITICAL REVIEW

The accurate use of impedance analysis for the study of microbial electrochemical systems

Xochitl Dominguez-Benetton,*[a] Surajbhan Sevda,[ab] Karolien Vanbroekhoven[a] and Deepak Pant[a]

Received 30th January 2012
DOI: 10.1039/c2cs35026b

The present critical review aims to portray the principles and theoretical foundations that have been used for the application of electrochemical impedance spectroscopy (EIS) to study electron-transfer mechanisms, mass transfer phenomena and distribution of the heterogeneous properties of microbial electrochemical systems (MXCs). Over the past eight years, the application of this method has allowed major breakthroughs, especially in the field of microbial fuel cells (MFCs); however, it is still most widely extended only to the calculation of internal resistances. The use and interpretation of EIS should greatly improve since the intrinsic knowledge of this field, and efforts and current trends in this field have already allowed its understanding based on rather meaningful physical properties and not only on fitting electrical analogues. From this perspective, the use, analysis and interpretation of EIS applied to the study of MXCs are critically examined. Together with the revision of more than 150 articles directly devoted to this topic, two examples of the correct and improved analysis of EIS data are extensively presented. The first one focuses on the use of graphical methods for improving EIS analysis and the other one concentrates on the elucidation of the constant phase element (CPE) parameters. CPEs have been introduced in equivalent circuit models, sometimes without solid justification or analysis; the effective capacitance has been obtained from CPE parameters, following an unsuitable theory for the case of microbial–electrochemical interfaces. The use of CPE is reviewed in terms of meaningful physical parameters, such as biofilm thickness. The use of a finite-diffusion element is reviewed throughout estimation of accurate values for obtaining the dimensionless numbers, Schmidt and Sherwood, in the context of a dioxygen-reducing-biocathode, under different flow-rate conditions. The use and analysis of EIS in this context are still emerging, but because of the promising potential of MXCs in renewable power generation, wastewater treatment and energy-positive biorefining, among other applications, it becomes necessary to boost our global capacities for the application of EIS—and especially its interpretation—so that we achieve a better understanding and optimization of these systems.

1 Introduction

Over the past decade, microbial generation of electric current was successfully achieved in the so called Microbial Fuel Cells (MFCs).[1–6] A more cost-effective application for electrochemically-mediated microbial production has been hydrogen generation in Microbial Electrolysis Cells (MECs).[7–10] More recently, in 2010 electricity-driven synthesis for the production of organic chemicals was first described in Microbial Electrosynthesis Cells (MESCs).[11–14] Microbial Desalination Cells (MDCs) demonstrated the possibility of reducing the salinity of an aqueous solution, while generating electrical power from electrolysis of organic matter.[15–17] Microbial hydrometallurgical cells (MHMCs) have been proven to be useful for copper recovery using the MFC concept.[18] Photosynthetic-MXCs have also shown progress.[19] Collectively, these technologies are referred to as Bioelectrochemical Systems (BESs) and, more particularly, Microbial Electrochemical Systems (MXCs) or Microbial Electrochemical Technologies.[20] They have received remarkable global attention,[21] especially because they can use complex solid waste or wastewaters as feedstock,[22–33] reduce energy-consumption compared to traditional processing,[34,35] and products can be generated with lower greenhouse emissions.[21] MXC technologies promise, as well, a big step towards energy-positive integrated biorefineries.[35]

[a] *Separation and Conversion Technology, VITO – Flemish Institute for Technological Research, Boeretang 200, Mol 2400, Belgium. E-mail: xoch@vito.be, xoch@xoch.info*
[b] *Department of Biochemical Engineering & Biotechnology, Indian Institute of Technology Delhi, Hauz Khas, New Delhi-110 016, India*

A MXC consists of an anode and a cathode, typically separated by an ion exchange membrane. At the anode, electrochemically active microbes oxidize organic or inorganic substrates using the electrode material as final electron acceptor.[12] Electrons are externally transported from the anode to the cathode where, in the presence of a suitable (bio)catalyst, they reduce oxidized species, sometimes into value-added products.[36] Contrary to MFCs, whose main product is electricity, for effectively achieving this process, MEC and MESCs (in many cases) need input energy. Spontaneously, in a MFC the anode potential (E_{an}) becomes lower than the cathode potential (E_{cat}). However, in MECs and MESCs, the thermodynamic barrier for product formation needs to be overpowered with an external power supply. In this way, E_{an} can be poised over E_{cat} so that the potential generated from substrate oxidation at the anode can be boosted to drive the cathodic reaction at high rates (Fig. 1). So far, the reaction of hydrogen evolution at the abiotic cathode is the foremost studied even without the use of precious catalysts *e.g.* platinum. Microbial cathodes have also been considered for CO_2 reduction to methane and multicarbon compounds.[11–13,37] The same general principle of operation is used for all other MXCs, except for MDCs where, instead of one or two compartments, an intermediate additional compartment is added for salt separation in an electrodialysis-like process.[15]

Interaction between electrodes and microbes can occur *via* direct electron transfer (DET) or mediated electron transfer (MET). In DET, microbial enzymes are set in such a way that electronic states in the surface material and enzyme active center (or other conductive structures) overlap, increasing the probability of electron transfer across the interface.[39,40] For this reason, DET kinetics is controlled by the electrode potential and by the closest distance between the surface[41] and electron transfer structures in the microbe. DET has been reported for about 40 redox enzymes[39] and a great number of bacteria, of which *Geobacter sulfurreducens* is considered the model organism[42] due to its ability to reach the electrode through conductive pili.[43]

In MET, natural or artificial electron transferring agents can readily participate in redox reactions of biological components.[44–48] MET has been reported for a great number of bacteria, of which *Shewanella oneidensis* MR-1 is considered the model organism.[49] Detailed lists of mediators can be found in previously published works.[44] Hydrogen can itself be considered as an electron shuttle for achieving MET.[50] Accessibility, suitable redox potentials, electrostatic interactions, pH and ionic strength are major factors that play a role in facilitating MET.

Electrochemically-active (EA) microbes have then been defined as those capable of producing electric current or exhibiting electron-exchange activity with a working electrode. Particularly, EA-biofilms have been recognized to play an important role in efficient electron transfer in MXCs.[51] Borole *et al.*[52] have recently provided a comprehensive review of EA-biofilm current status and future research needs. EA-biofilm-based processes do not occur uniformly and interpretation of data obtained through electrochemical characterization becomes complex due to—at least—heterogeneities and electron transfer mechanisms within.

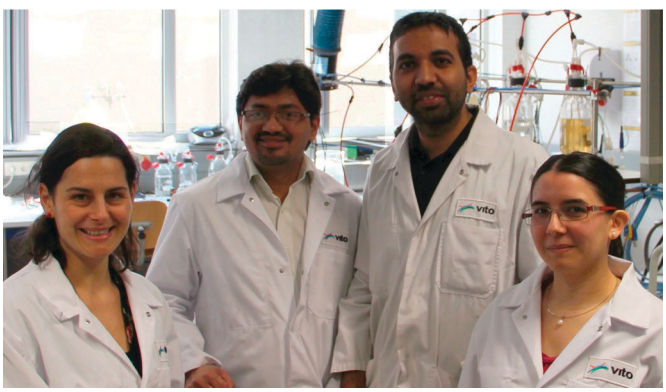

Karolien Vanbroekhoven, Deepak Pant, Surajbhan Sevda and Xochitl Dominguez-Benetton

Xochitl Dominguez-Benetton (DrSc) is a research scientist at the Flemish Institute for Technological Research (VITO) working on bioelectrochemical systems. She received her Doctor of Science degree from the Mexican Petroleum Institute, in biocorrosion. She has authored and co-authored 7 peer-reviewed publications related to the domain of bioelectrochemical systems, mainly biocorrosion, and two patent applications in microbial electrosynthesis. Her research experience lies in the application of electrochemical methods, especially Electrochemical Impedance Spectroscopy, to the study of microbiological systems and the use of the latter for electrochemical applications.

Surajbhan Sevda (MTech) received his Bachelor of Engineering in Biotechnology and Master of Technology in fermentation technology from University of Rajasthan and UDCT, University of Mumbai, India, in 2006 and 2008, respectively. He is currently in the third year of pursuing his doctorate degree in Biochemical engineering and Biotechnology from Indian Institute of Technology (IIT) Delhi at New Delhi with Prof. T. R. Sreekrishnan. His current research focuses on the microbial fuel cell development for wastewater treatment applications. Currently he is the visiting PhD student at VITO through Flemish government scholarship.

Karolien Vanbroekhoven (DrIr), Program manager at VITO, is responsible for the team of about 30 people involved in the program of industrial biotechnology and renewable chemicals in the unit of SCT. She has been involved as a partner/coordinator in several EU projects, national research projects and feasibility tests. She is an expert in bioconversion (like dark fermentation processes) and bioelectrochemical systems. She is responsible for the scientific program in the team as well as people and financial management.

Dr Deepak Pant is a research scientist at Flemish Institute for Technological Research (VITO) currently working on bioenergy, specifically, the design and optimization of bioelectrochemical cells for energy recovery from wastewaters and microbial electrosynthesis. He has a PhD degree in environmental biotechnology from TERI University, New Delhi (India), and has authored and co-authored 20 peer-reviewed publications (h-Index 10) and 8 book chapters to his credit. His research experience lies in industrial wastewater treatment, wasteland reclamation and restoration, biofertilizers, sustainable agriculture, biofuels and bioenergy and life cycle analysis (LCA).

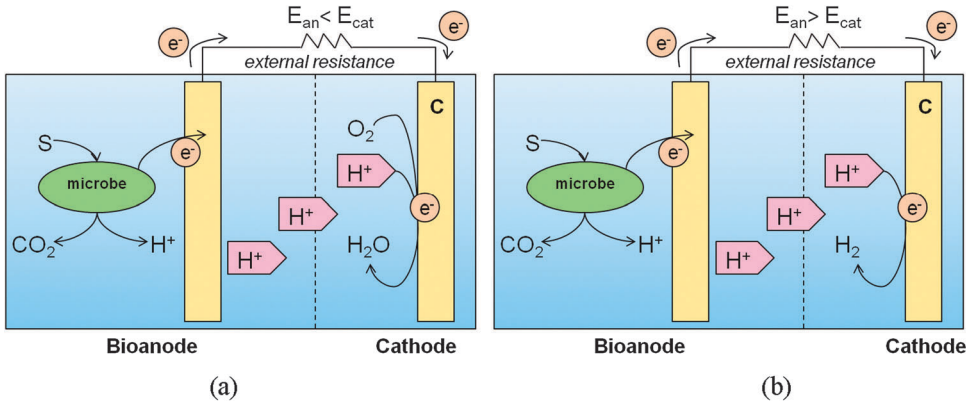

Fig. 1 General operation of (a) MFC, $E_{an} < E_{cat}$, (b) MEC, $E_{an} > E_{cat}$. In the MFC, at the anode compartment, oxidation of an organic substrate (S) to CO_2 can occur; however, other conversions are possible, such as sulfide to sulfur.[38] At the MEC cathode compartment, hydrogen formation is presented as an example of proton reduction to hydrogen formation; however, the reduction reaction at the cathode can consider the reduction of CO_2 to organics (MESC), N_2 to NO_3^-, Cl^- to ClO^-, U(VI) to U(IV), among others.[21] Electron (e^-) transfer to or from electrodes is microbially-mediated, in at least one compartment in the MXC.

The fact that MXCs involve electron transfer between bacteria and electrodes makes it possible to reveal current and potential relationships, which can be analyzed by different electrochemical methods. Most efforts to obtain such unique information have so far included chronoamperometry (CA),[53] cyclic voltammetry (CV)[54,55] and linear sweep voltammetry (LSV).[21] More recently, spectro-electrochemistry (SEC) has emerged as a novel approach for evaluating microbe–electrode interactions.[56,57] Illustrations of the application of these methods are as follows: setting the potentials of anodes and cathodes in MXCs by CA has allowed us to study the electrochemical microbial capabilities for extracellular electron transfer, and also to define optimal operational conditions for some systems, although most experimental setups have only used—and still do—a single potential.[58] Using CV, different sets of oxidation and reduction peaks have been revealed, showing that some microbes can discharge electrons at multiple potentials; also, the results of this technique have supported various types of mechanisms used for electron transfer, such as the use of mediators, direct contact through nano-wires and electron-transfer proteins or hydrogen as an energy carrier.[54,55,58–61] The polarization behavior of electrodes through LSV has mostly focused on estimating power production;[62] such behavior frequently shows power overshoot,[62,63] which can be avoided by running the bioelectrochemical reactor at a fixed resistance for a full fed-batch cycle.[62] The sophisticated Electrochemical Impedance Spectroscopy (EIS) has not been much applied to the study of MXCs, although it potentially provides extensive information.

The foundations of EIS can be traced more than a century ago, but it was not until the introduction of the "frequency response analyzer (FRA)" in the 1970s that the use of EIS was boosted as an analytical tool for electrochemical systems.[64] Over the past twenty years, detailed theoretical work has been developed for deriving the impedance functions for complex reaction mechanisms and mass transfer processes, as well as practical tools for assessing the viability and errors of impedance data.[64,65]

In the context of MXCs, the use of EIS has rapidly become relevant since 2004 (Fig. 2), due to the potential advantages it provides to their study. Despite its relevance, most research

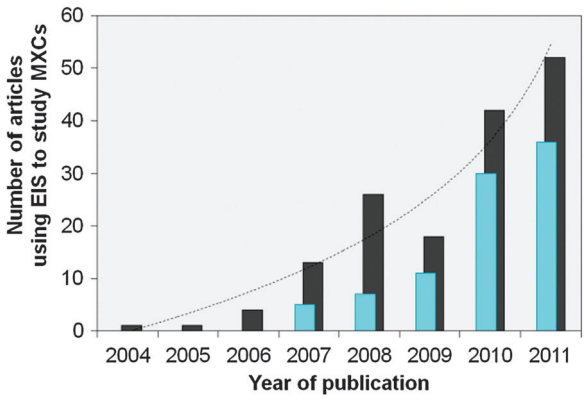

Fig. 2 Evolution in the use of EIS for the interpretation of MXC-associated phenomena. Black bars show the total number of articles published, to our knowledge; blue bars show those retrieved through the Science Direct search engine. A total of 157 articles were found for the period between 2004 and 2011, corresponding to about 1.2% of the more than 13 000 articles so far published on MXCs, since the discovery of MFCs.

applying EIS for MXCs has focused on a much simplified or erroneous application of the technique, and mostly rather basic analysis of spectra has been achieved to determine the internal resistances of a MFC.[63,66] Later on, efforts on its use to characterize electrode properties have been proposed.[63,67,68] The impedance data presented by these previous investigations were usually fit to equivalent electrical circuits (EECs). The constant phase element (CPE), widely described in Section 2.2.3 of this review, indicates a pseudo-capacitor-style element that introduces the distributed nature of an electrochemical interface; it has also been taken into account for these interpretations.[69–72] However, it is important to note that the assumptions implicit in the use of such electrical analogues and CPE may not be valid for a given experimental system and insight into the physical origin of the impedance responses may be lost when the interpretation of the spectra is limited to the use of such models.[65]

Progress in MXCs depends mostly on the elucidation of the limiting factors for power output in the case of MFCs,[73]

the hydrogen formation rate in MEC, or the kinetic rates and selectivity constraints for organic chemicals production in MESCs. Some of these limiting factors, as addressed by He and Mansfeld,[73] can indeed be represented by the internal resistances of the MXCs, but EIS is such a powerful tool that reveals a wider variety of chemical and physical processes. EIS measurements at the level of electrodes can also provide information on bacterial metabolism or electron transfer mechanisms, surface and material properties of the electrodes. Numerous studies have already incorporated EIS to investigate some of these aspects, but additional improvements on the advanced application and interpretation of EIS are undeniably necessary to make progress in the understanding and performance of MXCs.

In this review, efforts are made to provide stronger foundations for the analysis of data obtained for MXCs from the EIS technique, aimed at revealing physical meanings of some of the parameters that can be obtained. It is hoped that the works reviewed here will be helpful in understanding the structure and properties of microbial electrodes, but also they can offer practical ways for the analysis of EIS spectra obtained for MXCs, and present guidelines for extracting original meaningful parameters from the EIS results. As previously aspired by other authors,[73,74] we do expect a broader and better application and interpretation of EIS not only for MFCs but also for all kinds of MXCs, in the near future. To facilitate this process, we introduce illustrations of what is possible to be obtained with correct impedance analysis.

2 Electrochemical impedance spectroscopy (EIS)

The impedance response for even the simplest electrode–electrolyte interfaces often reveals a frequency dispersion of the data, which is generally attributed to the dispersion of the electrical properties of the interface.[75] Explaining the processes and phenomena occurring in MXCs, not only for those directly related to the electrochemical reactions per se, but also mass transfer phenomena, adsorption, (bio)chemical reactions preceding the electrochemical ones, biofilm and microbial growth, among others, then becomes complicated. The application of EIS to MXCs has its foundations on microbial-influenced corrosion (MIC)[76] and from there it has been extrapolated because it offers many advantages over other electrochemical methods, which include: (i) the use of a low-amplitude (non-intrusive) sinusoidal voltage that allows the system to remain at the pseudo-steady-state, (ii) rapid acquisition and quantification of some parameters, such as the ohmic resistance, film conductivity, diffusion coefficients, charge transfer reaction rates, (iii) accurate, repeatable measurements; (iv) high adaptability to different MXCs and (v) the possibility of characterizing interfacial properties in the presence and absence of redox reactions, as well as identifying separate phenomena in a single spectrum.[77]

2.1 Principles, theory and representations

EIS is a transfer function method.[78] The system under investigation is perturbed with an alternating wave input, commonly sinusoidal, and the response is measured at the output. If the system is linear, the response is also sinusoidal with the same frequency, but amplitude and phase vary. Electrochemical cells are not linear, nor are MXCs, *e.g.* doubling the input voltage does not necessarily doubles the output current; the property of the weighted sum of the response signal is not superimposed to the input weighted sum signal. However, in normal EIS practice, the amplitude of the alternating signal is sufficiently small (*e.g.* 1 to 10 mV) that usually the significant non-linear response of the cell to large imposed potentials is not observed and instead a pseudo-linear behavior is found. Non-linear systems generate harmonics (current and voltage variations) that modify the signal waveform, these can also be analyzed to estimate the curvature in the current–voltage curve of the cell.[64,79–81] Although interesting, focus on the analysis of harmonics is beyond the scope of this review; an appropriate introduction to this topic may be found in the work of Macdonald.[81] In order to avoid non-linear responses when measuring EIS spectra, prior inspection of the polarization curves to elucidate the correct settings has been proposed for MXCs.[74,82]

Besides linearity, other conditions for obtaining 'good' impedances are stability, causality and finiteness for all frequencies (from $\omega \rightarrow 0$ to $\omega \rightarrow \infty$). The system under study may not change with time while the EIS spectrum is being measured, nor continue to oscillate after the excitation is stopped, and the measured response ought to be solely due to the applied (perturbation) signal.[83] Sometimes, such conditions are difficult to be achieved and therefore measured data would then be corrupted. This all happens and cannot be fully avoided in slowly changing or aging systems,[83] as is the case of systems based on the use of EA-biofilms such as MXCs. Therefore, being able to discern between 'good' and 'bad' impedance data becomes of major importance for the validity of measured data. A few authors in the field of MXC have actually addressed these issues (explicitly or implicitly),[74,76,82] which should be a decisive concern for the use and interpretation of impedance.

A good tool for data validation are the Kramers–Kronig (KK) transforms,[74,83,84] which are mathematical relationships based on the principle of causality.[83] The KK transforms apply to all frequency-domain measurements which can satisfy the conditions of linearity, causality, stability and finiteness for all frequencies. Impedance data that do not satisfy the KK relations must violate at least one of the required conditions, however, satisfying the KK relations is a necessary but not sufficient condition to be met.[77] Besides direct integration of the KK relations, experimental, graphical and regression methods can be applied to check whether the impedance data meet the KK postulations.[74,77] The work presented by Strik *et al.*[74] provides some pertinent guidelines on the feasibility of EIS measurements and data validation, as well as a summary of the criteria for valid EIS results.

There are two standard graphical representations used in EIS. Complex plots, also called Nyquist plots, outline the real part of impedance (ReZ) *versus* the negative of the imaginary part (−ImZ); Nyquist plots should be presented with square axes to avoid vector deformation and consequential misinterpretations. Bode plots are frequency-dependent plots on the logarithmic scale (Fig. 3a and b). A direct study of these graphs would be the first advisable step toward the interpretation and assessment of impedance data. However, as obvious as it would seem, it is not the typical practice. For this reason, several authors have reported graphical analysis methods based on deterministic

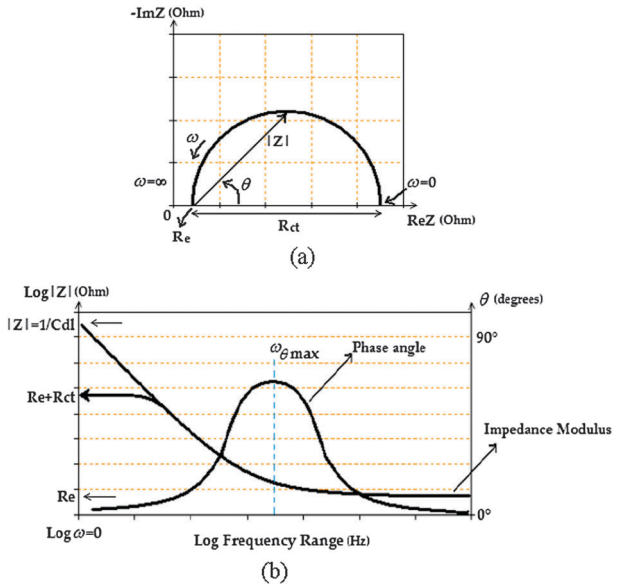

Fig. 3 Typical impedance response for an equivalent electrical circuit that consists of an active electrolyte resistance R_e in series with the parallel combination of the double-layer capacitance C_{dl} and an impedance of a Faradaic reaction, R_{ct}. (a) Nyquist plot: real impedance (ReZ) *vs.* negative of the imaginary impedance (−ImZ). (b) Bode plots of the impedance: phase angle (θ) and impedance modulus ($|Z|$) plots *vs.* frequency (ω) as an independent variable. C_{dl} stands for the double layer capacitance.

models out of the field of MXCs.[85] Using such methods, it has been demonstrated that the usual ways of representing impedance can be limited and more original graphical representations of EIS become quite useful. Examples of such representations are well detailed in the work of Orazem *et al.*,[85] although these approaches have not yet been employed in the context of MXCs. Further in this review, a comprehensible illustration of how to use these graphical methods is included.

Nyquist diagrams obscure the frequency-dependency (since frequency is not made explicit in such diagrams) as well as low-magnitude responses,[77,85] for which magnification of the high-frequency data is sometimes presented. The phase-angle Bode plots are sensitive to system parameters, thus providing a good means to compare modeled *versus* experimental data. However, in electrochemical systems where the ohmic drop is significant, its contribution to the total impedance complicates the detection of the electrode-surface phenomena in the phase-angle Bode plots. When it is possible to accurately estimate the ohmic drop contribution (electrolyte resistance), phase-angle plots can be ohmic-drop corrected, allowing detection of the existence of electrode-surface phenomena such as the CPE behavior, which otherwise would be obscure.[85] If an accurate estimation of the ohmic drop cannot be carried out independently of EIS data, cautious interpretation of the phase-angle ohmic-drop-corrected plots should be performed.

Impedance modulus Bode plots are less sensitive to system parameters, but the asymptotic values at low and high frequencies provide relevant information, such as electrolyte and charge transfer resistances (Re and Rct, as presented in Fig. 3). Therefore, analyzing this latter plot together with Bode-corrected plots can prevent misinterpretations regarding the ohmic-drop contributions. The imaginary part of impedance ImZ is independent of the electrolyte resistance, so data correction for this parameter is not necessary. For example, the CPE coefficient α can be directly obtained from the ImZ *vs.* frequency plots, as the slope of the curve above the relaxation frequency for the system.[85]

In summary, diffusion coefficients, Schmidt numbers, CPE parameters α and Q, among others can be extracted with relative ease from such representations.[85] While visual representation alone cannot provide all the explanation for the processes and phenomena occurring in MXCs, in principle it should provide new qualitative and quantitative insight into such systems. More details of the possibilities of these representations are given further in this article.

2.2 EIS applied to MXCs: state of the art

2.2.1 Internal resistances. The first publications on the application of EIS to MXCs, to our knowledge, account for measurements of the internal resistance (R_{int}) of MFCs.[86,87] It was determined that the internal resistance due to separators (*e.g.* proton-exchange membranes) represents a critical factor in the power density generated by a MFC.[87–89] Following these studies, a large amount of the focus of EIS in MXCs has been to determine only such internal resistances;[5,17,88,90–131] in many of these studies the cathode or anode was used as counter-electrode[16,71,88,90,91,93–96,107,132,133] and even as pseudo-reference electrode,[16,71,88,90–92,94–96,107,132,] respectively. It has been explained how R_{int} decreases by reducing electrode spacing which would seem classical for any electrochemical systems, but also power density was found to be reduced due to an increase of open circuit potential (OCP) of the anode electrodes.[90]

Using the principle of reducing electrode spacing, air-cathodes (gas-diffusion electrodes that conduct oxygen into an electrolyte) were proposed and proven to be successful in greatly reducing R_{int} of MFCs, as well as increasing power density,[134] reasons why they are now most widely employed.[118,135,136]

By using metallic current collectors (*e.g.* stainless steel mesh) pressed against the electrodes, R_{int} was also proven to be reduced.[95]

It has equally been found that when the system is not completely limited by high R_{int}, a good strategy for increasing power is to increase the anode surface area relative to that of the cathode; this is how brush anodes become influential, by showing low R_{int} while considerably increasing the anode surface area.[94]

Moreover, R_{int} has been measured for stacked-MFCs (single MFCs connected in series or parallel), compared to single- and two-chambered MFCs; this parameter is much lower for stack configurations making them an attractive alternative for MFC scale-up.[100,132] Also, it has been proposed that increased cation and anion transfer rates have an impact on R_{int} caused by concentration polarization (Fig. 4), the reason why the use of bicarbonate and phosphate buffers is extended as ion carriers in MFCs[92,93,110] and weak acids to enhance the hydrogen evolution in MECs.[137] Still, in order to avoid misleading comparisons between investigations, reporting internal resistance values referred to the projected electrode-surface active area is advised.

The intercept of the curve with the real impedance (ReZ) axis at the highest frequencies has been considered as the

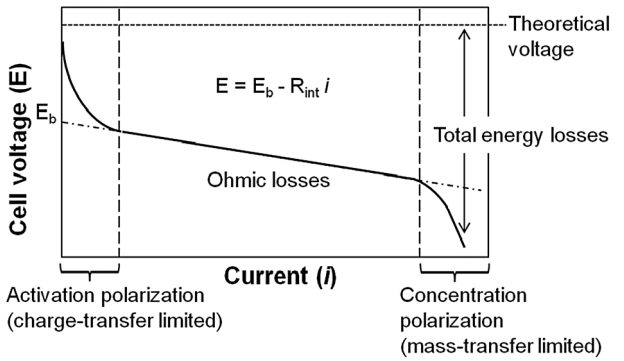

Fig. 4 Schematic representation of the ideal current–voltage polarization curve of a membrane-less MFC. The three regions of polarization overpotentials are shown: activation polarization, ohmic contribution and concentration polarization. Edited from Fan *et al.*[106] and Zhao *et al.*[82] Although important, the overpotential associated with preceding chemical or biochemical reactions, as addressed by Bard and Faulkner,[79] is frequently ignored from this considerations.

ohmic resistance (R_{ohm}) and the ReZ value of the lowest frequency (where ImZ = 0) has been considered as the total R_{int}. The difference between the total R_{int} and R_{ohm} is often considered the sum of charge-transfer (R_{ct}) and diffusion (R_d) resistances,[92] which together account for the polarization resistance. In summary, from this perspective, three types of resistances are commonly considered to contribute to $R_{int,}$ in MXC: R_{ohm}, R_d, R_{ct}, usually in that priority of significance. In this way, the internal resistance of a MFC has also been defined in terms of the anode and cathode polarization resistances by Manohar and Mansfeld[138] as described by eqn (1).

$$R_{int} = R_p^a + R_p^c + R_{ohm} \quad (1)$$

Although correct for membrane-less MXCs, its use in this arrangement has been less extended. Overall, R_{int} will encompass the activation or charge-transfer related (R_a^a, R_a^c) and concentration or diffusion-related (R_c^a, R_c^c) resistances contributing to the polarization resistance at both (bio)electrodes (a being the anode, c being the cathode), the ohmic resistance and the resistance of the middle components *e.g.* ion-exchange membranes (R_{mem}). Therefore, R_{int} is defined as in eqn (2), for a general MXC with an ion-exchange membrane in between the anode and cathode. Fan *et al.*[106] normalized the resistances by the projected areas of all components, being more precise for practical and objective comparisons.

$$R_{int} = R_{ohm} + R_c^a + R_c^c + R_a^a + R_a^c + R_{mem} \quad (2)$$

The importance of calculating the values of R_{int} and its components relies on their contribution to the cell performance. For example, in the case of a MFC, this contribution can be directly observed for the power density, P (eqn (3)).

$$P = E_b i - R_{int} i^2 \quad (3)$$

The parameter i refers to current density (A m^{-2}). E_b refers to the linear extrapolation open circuit voltage, this is the intercept of the linear curve (Fig. 4) with the voltage (E) axis; E_b should be close to, but less than, the measured OCP.

For numerous experimental results, all these resistances are not obvious to be obtained and modeling impedance data becomes necessary. R_{int} has been typically calculated by fitting the impedance data to EECs considered to be analogous to the MXC configuration.[90,93,98,139,140] These approaches have indeed allowed great advancement in the field of MXCs. However, careful application of EECs is necessary since theoretical misconceptions are easy to be made when using such electrical analogues. EECs explain a global impedance response that can be virtually represented by an infinite number of electrical passive element combinations.[141] This problem can be 'solved' when the electrical arrangement proposed (whose schematic representation has been omitted in various publications) has a physical explanation that is validated to represent the system under study.[81] Even so, EECs will still just provide an explanation of simple parameters that do not describe the distributed behavior of porous electrodes and interfaces with great heterogeneity,[142] such as biofilm-based systems.[141] To introduce the distributed-nature in such EECs, the CPE has been applied,[67,68,70,89,119] with further justification still required. A more detailed analysis regarding the CPE approach will be discussed later on.

EIS has been applied to measure R_{ohm} in MFCs and MECs, when the polarization curve is not linear and as a consequence a current-independent R_{int} cannot be straightforwardly defined.[5,117,137,143–150] It has also been applied to measure the resistance of different separators.[151] As expected for any electrochemical system, increasing R_{ohm} decreases the power output. The influence of R_{ohm} as a limiting factor in a MFC can be sometimes inferred from the shape of a power curve, giving a typical symmetrical semi-circle.[5] A characteristic frequency associated with R_{ohm} (ω_{ohm}) can be defined as expressed in eqn (4),

$$\omega_{ohm} = 1/(2\pi R_{ohm} C_{dl}) \quad (4)$$

where C_{dl} represents the double layer capacitance, indicating the frequency at which the capacitive current of an experimental system becomes limited by R_{ohm}.[77]

A MXC system with high R_{ohm} (*e.g.* 10 Ω cm^2) would obscure the behavior of the interfacial processes measured with EIS at high frequencies, reason why it is useful to include an oscilloscope in the experimental setup, capable of displaying Lissajous plots (which show the phase relationship between the sinusoidal EIS signals). So far, none of the works revised here have explicitly included an oscilloscope in the experimental setup, but by means of this instrument distortions in the elliptical shape can be detected for time-domain signals in the Lissajous representation of EIS, which are classical for high R_{ohm} systems. In applications other than MXCs such behavior has motivated the use of R_{ohm}-corrected Bode plots, but these must be interpreted cautiously.[77]

When possible, an estimation of R_{ohm} should be made independently of regression with EIS data (*e.g.* using the current-interrupt technique) to avoid misinterpretations due to the manifestation of bogus high-frequency relaxation processes.[5,77] Nonetheless, sometimes it is rather challenging to extract meaningful information from the non-corrected traditional Bode plots, when the R_{ohm} cannot be neglected. Besides, R_{ohm}-corrected

Bode plots can be used to identify CPE behavior at high frequencies and to properly extract values for the CPE coefficient α. With the knowledge of α, the parameter Q is easy to determine by using eqn (5).[77]

$$Q = (-\sin(\alpha\Pi/2))/(\mathrm{Im}Z\omega^{\alpha}) \quad (5)$$

As considered when applying a CPE to explain the global impedance of an electrochemical interface, a geometry-induced distributed behavior would imply the existence of not only distributed current and potentials but also distributed local ohmic impedances $R_{ohm,loc}$.[77] Local-EIS has been found to provide a good means for assessing the influence of local variations on the CPE behavior seen in global impedance measurements;[75] this approach has not yet been extended to the study of EA-biofilms in MXCs, however it has been applied to MIC studies.[152] In general, MXCs do have high global R_{ohm}, which is inconvenient for practical applications, especially because they account for a significant amount of the total cell voltage.[143]

The impedance spectra of different microbial anodes have besides been constructed for characterizing the substratum-material performance, *e.g.* composites, materials modified with carbon nanotubes (CNTs), conductive polymer composites, or both. In the case of conductive polymer-doped electrodes, quite well-defined semicircle behaviors with fairly poor diffusion control are usually found over a broad frequency range. Spectra of such electrodes seem to almost only vary in terms of charge transfer resistance R_{ct}, which is usually associated to the inverse of the electrochemical reaction rate. R_{ct} has proven that both CNTs and polyaniline (PANI), and more strongly CNT–PANI composites, functionalize carbon-based electrodes in such a way that the charge transfer rate is improved mainly due to an increase in the specific surface-area. In the presence of bacteria, such an effect is significantly magnified.[153–156] However, for electrodes of different nature, studies have shown that specific surface area is not the single variable explaining the differences in R_{ct} (and current density).[70]

Currently, the internal resistances are often described as power or energy losses[68,157,158] and their individual contributions (Fig. 4) can be successfully delineated, after the first insertion of reference electrodes for achieving more reliable impedance measurements in MXCs.[68,76]

2.2.2 Kinetic limitations and the polarization behavior. EIS has been applied additionally for the detection of the environmental limiting processes in MXCs, such as the effect of pH and biofilm formation on the electrodes.[154,159]

For instance, EIS has been measured separately for the anode and cathode interfaces in MFCs, showing that—under certain environmental conditions—the cathodic reaction can be the limiting factor, observed as a higher contribution of $R_{ct} + R_d$ (the polarization resistance) to the total impedance. Such behavior has been found to be importantly affected by pH. While air-cathodes can tolerate high pH values (*e.g.* 8–10), the EA-biofilm activity and the oxygen reduction reaction are pH-sensitive and, by themselves, these processes can have an influence on pH by supplying or consuming protons. Therefore, under optimal pH conditions for bioanode development, the polarization resistance of the cathode increases, demonstrating its limiting behavior. Otherwise, rising pH for improving the cathodic reaction can become limiting to the anodic biofilms. The performance of both the anode and cathode is determined by the mixed effects of the anolyte and catholyte pH on both the anodic and cathodic reactions,[159] and consequently on EIS measurements. The conditions of MECs, MESCs and other types of MXCs would have different pH needs; however, the pH dependency remains high and optimal conditions for the operation of bioanodes or biocathodes still need further elucidation for these systems, as well as their impedance response.

The microbial biofilm itself is a kinetic-limiting factor. For example, using pure cultures *versus* microbial consortia would directly influence the surrounding conditions of the electrode material; furthermore, the electron-transfer mechanisms would not be the same.[58] For example, the polarization resistance, predominantly influenced by R_{ct} in MXC using conductive polymer composites,[153,154,160,161] is affected by the nature of the electron-transfer mechanisms predominating in the biofilm. While a biofilm formed only by *G. sulfurreducens* would show high anodic reaction rates due to direct electron transfer possibilities, microbial consortia operating in the same MFC configuration and under the same operational conditions would show higher R_{ct}, even if the conductivity of the electrolyte is highly improved (*e.g.* from 10 to 50 mS cm^{-1}). The effective capacitance has also shown to differ from one EA-biofilm to another in the same type of MXC. In the presence of microbial consortia, the effective capacitance C_{eff} has been suggested to be larger than the one for pure *G. sulfurreducens* biofilms; this was attributed to a good surface conditioning by the complex biofilm, creating a higher proportion of potential active sites for charge transfer reactions to occur. Nonetheless, *G. sulfurreducens* effectively outcompetes in better power density performance,[154] perhaps after its proven capabilities for direct electron transfer to a wider distance than only that available at the electrode surface.

The polarization behavior of a pure culture that performs mediated-electron transfer has also been studied. The polarization resistance has been considered to be inversely proportional to the reaction rate. For particular pure cultures, *e.g. Shewanella oneidendis* MR-1, the impedance spectra, together with other electrochemical methods, demonstrated how the addition of MR-1 increases the rate of substrate oxidation at the anode. The effective capacitance, at the anode level, for this case showed to slightly increase in the presence of the bacterial strain.[63] Analysis of the capacitance obtained for an MR-1-based MFC was further explained, a higher capacitance for the cathode than for the anode, as due to a higher active surface area of the Pt-plated graphite cathode.[76]

Ramasamy *et al.*[68] employed eqn (6) for describing a single or multistep electron transfer mechanism.

$$R_{ct} = RT/nFi_{ex} \quad (6)$$

R is the gas constant in J mol^{-1} K^{-1}, T is the temperature in K, n is the number of electrons involved in the charge transfer reaction ($n = 8$ for acetate oxidation), F is the Faraday constant (C mol^{-1}), and i_{ex} is the exchange current density for the electrochemical reaction. The use of this equation has allowed us to obtain kinetic rate constants or exchange current

densities for bio-electrochemical substrate oxidation during initial biofilm development, proving severe kinetic limitations that play an important role in the overall power output of a MFC. Despite these efforts, mechanistic analysis through EIS models has not been extended to the field of MXCs.

On the other hand, the combination of set anode potentials and terminal respiratory enzymes used by certain exoelectrogenic bacteria not only affects the electron-transfer rates but also the electron transfer mechanisms in MXCs. An example provided by Wagner *et al.*[58] states that if a microbe can only adjust its respiratory enzymes to low potential and the electrode is poised at a higher potential, then the microbe will only be able to capture part of the total available free energy. It is anticipated that the additional free energy between the terminal respiratory enzyme and anode potential is wasted. With a combination of CV and EIS (analyzing the polarization resistance), it was proven that the current generation performance is indeed improved at lower potentials for some bioanodes.[58]

However, due to the nature of the impedance diagrams obtained by such studies (one time constant with no significant diffusional limitations), the polarization parameters were still obtained by fitting the impedance data with classic electrical analogues.

2.2.3 CPE and the effective capacitance. It has been shown that the electrodic-biofilm formation affects not only the resistances in the MXCs, but also the pseudo-capacitive behavior.[71,119] The distributed nature of the properties that describe the reactivity of electrochemical systems is often represented in EECs with a CPE.[162] Mathematically, the impedance of a CPE describing a blocking system is represented by eqn (7).[163]

$$Z_{CPE} = 1/((j\omega)^{\alpha}Q) \quad (7)$$

Here, j is the imaginary unit ($j^2 = -1$) and ω is the angular frequency ($\omega = 2\pi f$, f being the frequency in Hz).[75] The CPE parameters Q and α are frequency-independent constants; Q represents the differential capacitance of the interface when $\alpha = 1$; when $\alpha < 1$ Q cannot represent the capacitance.[162] The dimensionless parameter α is related to the angle of rotation of a purely capacitive line on the complex plane plots.[75] The CPE has been considered to represent a circuit parameter with limiting behavior as a capacitor for $\alpha = 1$, as a resistor for $\alpha = 0$, and as an inductor for $\alpha = -1$.[75] For this reason, the CPE is used as a quite flexible parameter for fitting impedance data; however, the physical meaning of the processes underlying such a response cannot be clarified from just the purely mathematical description that a CPE model represents.[163]

Two major concerns with the use of CPE models, after the work of Orazem and Tribollet,[77] are: (1) at first sight an impedance response may appear to have a CPE behavior, but the frequency-dependency of the phase angle may show contradictory performance, as the time-constant is in fact not a constant but a parameter that follows a specific distribution which could resemble that of a CPE, and (2) a satisfactory fit of a CPE-based model to experimental data may not be correlated to the physical processes that govern the system, thus not guaranteeing that the model describes it correctly. To avoid this, the CPE parameters can be estimated graphically—in a given frequency range—from the Bode plot for imaginary impedance, as described by Orazem *et al.*[85]

The use of CPE in EECs has already been extended to model the impedance response of MXCs, basically due to their porous (bio)electrode-nature.[67,68,70,71,89,117,119,121,164–168] In most studies the use of the CPE is unjustified or given without supplementary information on its significance. Capacitance values have been extracted from such CPE data. The studies by Ramasamy *et al.*,[68] Jung *et al.*,[67] and Borole *et al.*[72] took the units obtained for Q as the same for the double layer capacitance (Farad s cm^{-2}), which would only be valid if $\alpha = 1$; Q is a constant with dimensions ohm cm^2 $s^{-(1-\alpha)}$ [75] or F $s^{(\alpha-1)}$ cm^{-2}, and not simply Farads.

Several examinations of the relationship between CPE parameters and the interfacial or effective capacitance (C_{eff}) have been explored. Hsu and Mansfeld (HM)[169] proposed eqn (8), where C_{HM} is the interfacial capacitance (F) and ω_{max} (or K_{max}) the angular frequency at which a maximum imaginary impedance magnitude is obtained.

$$C_{HM} = Q\omega_{max}^{(1-\alpha)} \quad (8)$$

Nonetheless, the hypotheses of Hu and Mansfeld for this approach[169] remain unclarified.[170] The study of Cordoba-Torres *et al.*[170] recently demonstrated that for a 2D distribution, the electrolyte resistance must be considered (as in the equation developed by Brug *et al.*,[171] further described in this review). For this reason, the C_{HM} equation could be considered only if the measured impedance corresponds to that of a 3D layer. Moreover, even in the case of a 3D layer, such equation would stand valid only for a certain situation, for example, it would be inconsistent for the description of systems in which there is no association between the resistance- and the CPE-analogous phenomena. A comprehensive explanation of such a situation has been provided in the work of Cordova-Torres *et al.*[170]

The studies of ter Heijne *et al.*[70,172] used this approximation (eqn (8)) to describe the behavior of bioanodes and biocathodes in MFCs. However, it should be first noted that such an equation is based on the model of a CPE in parallel with a charge transfer resistance, and may not even exist for other experimental cases. The effective capacitance C_{HM} can also be described as presented in eqn (9), where R_f represents the resistance of a film.[169]

$$C_{HM} = Q^{1/\alpha}R_f^{(1-\alpha)/\alpha} \quad (9)$$

Therefore, despite the extended application of the HM-equations to estimate the capacitance of many electrochemical interfaces, limitations of their applications have been found recently,[163] concerning (at least) the conditions of validity when representing a surface or a normal distribution of the time-constants.

The effective capacitance C_{HM} is meant to explain a normal time-constant distribution through a surface layer (Fig. 5a).[162] For such a case, the global impedance of the electrochemical interface can be simplified as a Thévenin equivalent from the additive (normal) contributions from each part of the layer (Fig. 5a). Such electrical equivalent would consider a global ohmic resistance in series with the summation of the impedances of the Voigt R_iC_i elements, represented in terms of a CPE in

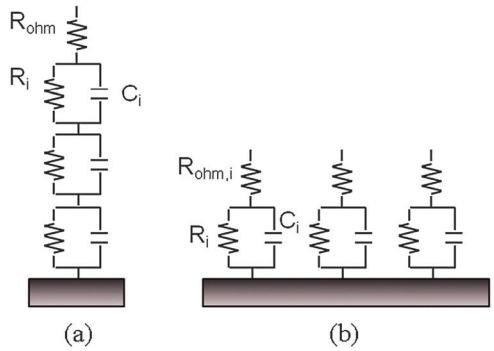

Fig. 5 Representation of different distributions of time-constants that may be represented by a CPE. (a) Normal distribution and (b) surface distribution. The ohmic resistance (R_{ohm}) is taken globally for the normal distribution and local ($R_{ohm,i}$) for the surface distribution. The distribution of the time-constants R_iC_i can be respectively observed for the two distributions. Modified from ref. 162.

parallel with the film resistance R_f. Distributions of time-constants for EA-biofilms distributed along the surface of an electrode would naturally entail distributed physical properties. Normal-distributions of time constants are usually expected in systems involving dielectric- or conductive-system dispersion, such as oxide films, organic coatings and human skin.[173] Also, normal-distributions are expected in systems with distributed porosity or surface-roughness.[77]

The intuitive association of microbial biofilms with organic coatings may lead to the conception of EA-microbial biofilms as conductivity-dispersed. As it is, the dispersion of conductivity within biofilms has not yet been clarified. However, it was recently published that biofilms made of different kinds of microbial species and even different kinds of strains of a single species can differentially influence the conducting or insulating nature of the film.[174] Therefore, on the side of being highly porous and rugose, it could be suggested that an EA-biofilm formed by multiple microbial species would have its conductivity dispersed at least as a function of the microbial-diversity concentration gradients. However, normal-distribution-based calculations of the effective capacitance made for single-species-based MXC-interfaces[70] or homogeneously distributed biofilms should still be cautiously reproduced.

Moreover, calculations made using the C_{HM} equation should be avoided as there is solid proof that the normal-distribution-based effective capacitance cannot be estimated only from the characteristic frequency and the semicircle-diameter magnitude as the C_{HM} equation proposes, but from the physical properties of the film itself, as anticipated by the power-law model developed by Hirschorn *et al.*[173] and represented in eqn (10),

$$C_{eff} = (\varepsilon\varepsilon_0/\delta)(1/g)(\rho_0/\rho_\delta)^{1-\alpha} \quad (10)$$

where a distribution of resistivity provides the boundary restrictions at the interface, ε being the dielectric constant, ε_0 the permittivity of vacuum (8.8542×10^{-14} F cm^{-1}) ρ_0 and ρ_δ the boundary values of resistivity at the interfaces, δ the thickness of the layer, and g a numerically-evaluated function[163] represented by eqn (11).

$$g = 1 + 2.88(1 - \alpha)^{2.375} \quad (11)$$

Otherwise, time-constants (RC) may be surface-distributed on the electrode (Fig. 5b). The deterministic expression that has been widely employed to describe the effective capacitance for such distribution, represented by eqn (12), was developed by Brug *et al.*[171]

$$C_B = Q^{1/\alpha}(R_{ohm}{}^{-1} + R_{ct}{}^{-1})^{(\alpha-1)/\alpha} \quad (12)$$

Surface-distributions of time constants anticipate systems where R_{ohm} significantly contributes to the impedance response. In the absence of R_{ohm} such systems are not expressed in terms of CPEs but in terms of an effective *RC* occurrence, thus for a surface-distributed CPE-associated behavior $R_{ohm,i}$ is required. An example of this type of geometry-dependent distribution has been suggested for the ideally polarized blocking electrode.[162]

The effective capacitance in electrochemical systems is sometimes used to estimate the thickness of dielectric layers. The power-law model can estimate with high accuracy such thickness for a wide variety of systems,[163,173] validating the effective capacitance estimations. The C_B equation calculates with more accuracy the effective capacitance or surface-distributions (when compared to C_{HM} for normal-distributions), but still needs further improvement for film-thickness calculations. The capacitance (under valid limits) relates to the film thickness (d_{eff}) as expressed in eqn (13).

$$C_{eff} = \varepsilon\varepsilon_0/d_{eff} \quad (13)$$

As observed, if the film thickness is calculated from an inaccurate value of C_{eff} (*i.e.* C_{HM}), the value obtained can significantly differ from the real thickness.[162] Although estimating the film thickness might be the most extended end-use for the effective capacitance calculations, other applications underlying inaccuracy of the same nature are expected. For instance, qualitative comparisons (based on C_{eff}) of the degree of electrode roughness and resulting surface area have already been suggested for MFC bioanodes.[70] So, in the use of EIS to study MXCs, the application of CPEs to model the impedance data and subsequent calculation of the effective capacitance would preferably involve becoming aware of the applicability of at least the equations concerning a normal—or surface—distribution of the time constants on the electrode under study. The selection of the proper equation rests on the knowledge of the system under investigation, obtained by the use of complementary characterization techniques. Of course, this problem is not only characteristic of MXC systems and the recommendations made here can be extended to the use of EIS for the characterization of non-EA microbial biofilms as well as enzyme-based electrodes, among other applications.

Otherwise, the capacitance can be obtained without the use of a CPE model. For example, the Mott–Schottky technique can be applied, by measuring EIS at a fixed frequency as a function of the direct current (DC) potential, as given by the Mott–Schottky relationship (eqn (14)), where C_{SC} is the capacitance of the space charge region (continuum of distributed charge), N is the donor density (electron donor concentration calculated from the slope $1/C^2$ *vs.* E_{WE}, with E_{WE} as the potential of the working electrode), E is the applied

potential, E_{FB} is the flatband potential (determined by extrapolation to $C = 0$ of the slope $1/C^2$ *vs.* E_{WE}), C is the capacitance, and k is the Boltzmann constant.[175]

$$1/C_{SC}{}^2 = (2/e\varepsilon\varepsilon_0 N)(E - E_{FB} - kT/e) \qquad (14)$$

The potential fixed-frequency EIS would provide information about the charge-transfer and adsorption mechanisms. However, the Mott–Schottky technique masks the CPE effect. In the presence of a CPE, if the Mott–Schottky formula is applied at different frequencies, different results are obtained. Then in the presence of a CPE, from the Mott–Schottky technique only a qualitative result can be obtained.[77] The best method is to determine the CPE for each potential and to try to extract C_{eff} before applying eqn (14).

Besides, this method can be applied only when the frequency selected allows full differentiation of the phenomenon of interest.[77] According to Orazem and Tribollet,[77] the Mott–Schottky analysis is only applicable in a restricted potential range for some systems, besides there should be no leakage current or Faradaic reaction to allow charge transfer across the electrode–electrolyte interface, unless the measurement is taken at sufficiently high frequency where the effect of Faradaic reactions is suppressed. For this reason, this method is more frequently applied in the context of semiconductor interfaces. Nonetheless, this approach has been applied in the context of MXCs to show the formation of an n-type semi-conducting layer over stainless steel anode materials at certain potentials, which is considered detrimental to the occurrence of the anodic processes. Such a layer was disrupted under open circuit-conditions, enabling the efficiency of the MFC to be restored.[175]

2.2.3.1 Localized electrochemical impedance spectroscopy (LEIS). It was shown that a CPE is extensively used in modeling the frequency response of MXCs. The CPE behavior is generally attributed to normal or surface distributed time constants, related to heterogeneous surface reactivity, roughness, electrode porosity, and to current and potential distributions associated with electrode geometry.[75] A wide variety of AC and DC methods have been developed for examination of the local events in electrochemical interfaces. Examples of these methods have been elsewhere described,[176] including Scanning Reference Electrode Technique (SRET), Scanning Vibrating Electrode Technique (SVET), Scanning Electrochemical Microscopy (SECM), Scanning Kelvin Probe Microscopy (SKPM), Scanning Kelvin Force Microscopy (SKFM) and Localized Electrochemical Impedance Spectroscopy (LEIS). Depending on the type of information required (mechanistic, topographic), each of these methods may provide advantages or disadvantages. When considering characterization of the distribution of local electrochemical events, and their nature, LEIS has been proved to be an efficient tool.[176–179]

In classical EIS measurements, the impedance response of the electrode is generally pointed out at the overall projected surface of the electrode in MXCs. As addressed in this article, electrochemically-active microbial biofilms enclose high heterogeneity and a more accurate approach to elucidate how time constants are distributed in these systems would indeed require a localized approach as LEIS could provide. As previously explained by Frateur *et al.*,[177] a global frequency response considers averaged measurements of potential and current. In contrast, the local impedance (Z_i) considers the ratio of a local potential perturbation to the local current density, measured at the same location. The LEIS is obtained from local alternative currents which can be deduced from potential gradient measurements using two platinum electrodes positioned above the surface under study.[180]

LEIS has been extensively used for understanding localized corrosion phenomena, including MIC.[177,179,181] The size of the electrochemical probes used for this purpose is a critical factor in achieving convenient spatial resolution; micro-reference and counter-electrodes are generally used. The foremost advantage of LEIS is being both spatially and frequency-resolved, which allows mapping the reactivity of different points over an electrode surface over a whole frequency range.[180] Two-electrode micro-probes (bi-electrode) are so far the most common technique to generate LEIS data,[182] although vibrating probes and microcapillary-based methods have also been studied.[180] The interfacial impedance Z_i can be represented by the sum of local interfacial impedance $Z_{i,0}$ and local ohmic impedance $Z_{ohm,i}$.[77] Local impedance mathematical expressions are described in the work of Lillard *et al.*[182]

Although LEIS has not yet been applied in the context of MXCs, it is here recommended as a suitable tool for discerning the nature of time constant distributions in electrochemically-active biofilm based MXCs. In this way, an accurate mathematical approach for calculating the global effective capacitance (and even its localized contributions) may be judiciously selected, when necessary.

3 The future of EIS analysis for MXC interpretation

The previous sections of the present article focused on reviewing the works that have been carried out in the context of MXCs, where impedance is applied as a tool in their studies. Some of the information already reviewed provides some guiding threads for the use and interpretation of EIS in MXCs. For example, the need to properly select an EEC or to better justify the use of CPEs was already pointed out. The use of LEIS measurements was suggested as a suitable approach for future understanding of electrochemical mechanisms or phenomena in MXCs, as well as the localized processes occurring within. The use of graphical methods in the interpretation of impedance data was also recommended, after the work of Orazem *et al.*[85] The calculation of effective capacitances was examined in terms of the applicability of the equations usually applied for this purpose. Besides, the article presented by He and Mansfeld[73] already provided some useful suggestions to be explored beyond the estimation of internal resistances.

Some of these approaches have been available in the scientific literature provided by EIS specialists. Many ways to analyze EIS data are not novel and some of them were even published more than 20 years ago.[183] However, these approaches have not yet been adopted in the field of MXC as it is an emerging research field, especially because most MXC specialists are only initiating the comprehension of EIS and its underlying theoretical grounds while the state of the art of EIS analysis and interpretation is already far too complex for the general researcher.

Without any doubt, the field of EIS is intricate but this should not be a reason to neglect its advances and fundamentals. Due to the understanding of this complexity the present section illustrates how to explain EIS data obtained from correct measurements in MXCs. For this purpose, some examples are provided with the objective of presenting what can be obtained with a correct and improved analysis of EIS data.

3.1 How to explain EIS data from measurements in MXCs?

EIS is not a stand-alone tool for the analysis of electrochemical systems. It is the application of a frequency-domain measurement to complex systems that cannot be explained straightforwardly,[77] including MXCs. What is obtained with this technique is not a direct measurement, but an indirect view of the influence of the physico-chemico-biological properties that actually explain the processes and phenomena occurring within the systems under study. Therefore, EIS cannot be applied in isolation, but in combination with other analysis tools and by using the former knowledge that has been already clarified.

While at this point there is no doubt that EIS is a very powerful tool for the analysis of electrochemical processes and that it is becoming a very powerful tool for the analysis of MXCs, it has also become evident that scientists and engineers participating in the progression of this line of work find the experimental data to a certain extent incomprehensible and most of the time do not pursue further analysis other than simplistic calculations of individual parameters (*e.g.* estimation of internal resistances).

Based on the previously reported MXC experimental results and relevant EIS literature, we provide here from a critical perspective a set of illustrations of how to correctly analyze EIS data. However, it must be remembered that no single path exists to explain every data series obtained from EIS measurements and for this reason, at least, interaction between MXC and EIS specialists is essential to improve the analysis thereof.

3.1.1 Improved graphical representations of EIS data. As previously mentioned, the general approach to represent EIS data for the study of MXCs has been the use of only Nyquist and Bode diagrams for phase angle and impedance modulus; nonetheless, the method of choice for this representation will also have an impact on the way data are visualized and might prevent us from noticing additional valuable information about the system under study. For instance, here we review in detail EIS results provided in the work of Aaron *et al.*[71] in which, among other aspects, the effect of ionic strength on the performance of an air-cathode microbial fuel cell was assessed. A Nyquist plot was presented by the authors of the original work, varying anode-fluid ionic strength. The initial ionic strength of a nutrient medium containing mineral salts and trace metals was 0.37 M, which was diluted with distilled water to obtain lower strength solutions 0.19 M (50%), 0.093 M (25%), and 0.037 M (10%), respectively. The applied AC signal for EIS was 1 mV rms and had a frequency range from 100 kHz to 100 mHz, with ten points per logarithmic decade.[71] We illustrate here how these impedance data could be shown in different representations. Fig. 6a shows the impedance data as exposed in the original article; however, square-scaled axes are introduced (the unit scale has exactly the same length for the real coordinate in the abscissa axis as for the imaginary coordinate in the ordinate axis), normalization to electrode area is presented, and distinction of some frequencies is placed to simplify visual examination. Magnification to high frequencies is also presented (Fig. 6b), as a means to verify the appearance or non-existence of characteristic phenomena in such a range. This way to present complex diagrams is the foremost approach accepted by the EIS scientific community and is preferred to be used for standardization and accuracy purposes.

As Aaron *et al.* pointed out, it is readily evident that R_{ohm} (intercept of the curve with the ReZ axis at the highest frequencies) is inversely related to the salt concentration (higher salt concentration means lower R_{ohm}) and, as a consequence R_{int} becomes affected.

On the other hand, the same authors[71] anticipated a model (based on EECs) containing—among other electrical passive elements—two constant-phase element contributions to the full-cell impedance response, representing the anode and cathode electrical double layer capacitance, respectively. Although appropriate, this choice was not justified in terms other than providing a generic explanation for the electrical

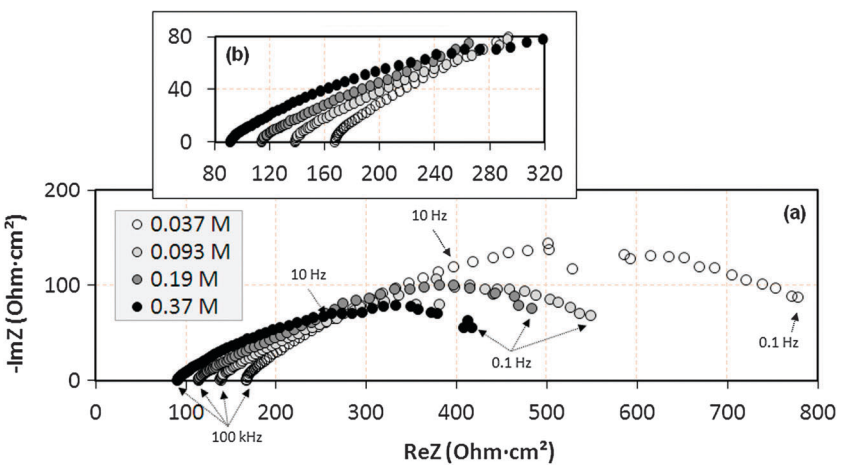

Fig. 6 Impedance plots of varying anode fluid ionic strength experiments, reconstructed from the work of Aaron *et al.*[71] (a) Full frequency range (100 kHz to 0.1 Hz). (b) High-frequency magnification (100 kHz to 10 Hz).

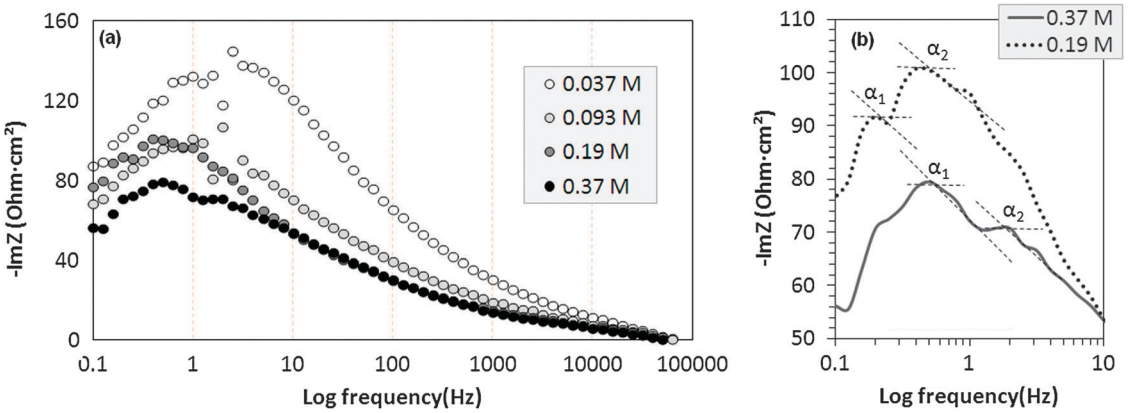

Fig. 7 Bode plots of imaginary impedance obtained after varying anode fluid ionic strength, reconstructed from the work of Aaron *et al.*[71] (a) Full frequency range (100 kHz to 0.1 Hz). (b) High-frequency magnification (10 Hz to 0.1 Hz). Note that for both ionic concentrations (0.037 M and 0.19 M), one α indicates a relative, while the other is the total maxima for the full frequency range and therefore not limited to the interval between 0.1 to 10 Hz.

passive elements proposed—still, this and other articles of the same research group are among those of better quality in the field of EIS applied to the study of MXCs.

One of the preferred preliminary steps before modeling EIS data would be examination of the graphical outcome, with the purpose of analyzing the overall nature of the system. For example, the imaginary part of impedance as a function of frequency, shown in Fig. 7a, readily allows identification of peaks appearing at characteristic frequencies, independently of the effects of the electrolyte resistance R_{ohm}. Observation of multiple maxima shows that data must be interpreted in terms of more than one process,[77] according to the characteristic frequencies at which they are observed. Fig. 7b spotlights two relative maxima (obtained from the *sign change in the derivative* of -ImZ with respect to frequency) encountered at frequencies between 0.1 and 10 Hz for spectra at 0.19 M and 0.37 M ionic strength, implying that there are at least two controlling processes within the system. Therefore, the use of two CPEs would be valid only if for the two processes detected $\alpha < 1$. Departing from the maxima encountered, the values of α_1 and α_2 were estimated for the curves obtained at 0.37 M ($\alpha_1 = 0.97$, $\alpha_2 = 0.91$) and 0.19 M ($\alpha_1 = 0.86$, $\alpha_2 = 0.84$), being for both cases $\alpha < 1$.

Therefore, one can consider that the explanation of such curves with two constant phase elements included in the model proposed by Aaron *et al.*[71] is accurate for the frequency range studied. Moreover, the values obtained for α suggest a more homogeneous distribution of the local properties of the electrochemical interface as the ionic strength of the electrolyte is higher. More insight on this type of analysis of impedance spectra was addressed in the work presented by Devos *et al.*[184] Data for ionic concentrations of 0.037 M and 0.093 M were excluded from this revision, due to the presence of some points in disagreement with Kramers–Kronig transforms in the frequency range of interest, however such data are still considered to be globally consistent with a two-process mediated system.

The values of α can be later on used to obtain an apparent effective capacitance, as described by Orazem and Tribollet,[77] and as presented in eqn (5) of this review.

Certainly, using the graphical method approach to analyze the data presented by the original authors does not oppose or invalidate their analysis, especially as it is here presented as an illustration of how to enhance data interpretation. For other cases, this type of analysis (if correctly applied) may reveal new phenomena and processes occurring in a MXC.

This type of interpretation is considered to be a first step to explain the EIS response. It can be applied to purposes other than obtaining the time constants and α parameter of a CPE. Graphical methods have lead, as reported by Tribollet *et al.*,[183] to direct extraction of Schmidt numbers from experimental data, where the convective diffusion impedance dominates. This method is approached in the next section of the present review, as a means of connecting the knowledge obtained in other fields of application of EIS to the domain of MXCs. Another example of this method is the assessment of impedance data at different temperatures, revealing the influence of a single dominant activation-energy controlled system by graphical superposition of impedance data.[85]

What is most important to consider is that as a result of only expanding the graphical varieties of the obtained data it is already observed that EIS results can be better justified and explained, and this approach can be readily used as a strategy to start explaining the frequency response of MXC.

3.2 Model-based graphical methods: beyond the use of physically-unjustified electrical analogues

A recent work developed by ter Heijne *et al.*[172] identified physical parameters related to biocathodes in a flow-controlled experiment using EIS and explained its response with a CPE/Z_d-based model, where Z_d represents the diffusion impedance. Experiments were performed after changing the flow-rate (ν) of the peristaltic pump between 0 and 80 rpm, resulting in linear flow rates between 0 to 2.8 cm s^{-1}. The thickness of the diffusion boundary layer was calculated by these authors, based on eqn (15), with ω_D as the diffusion frequency related to the diffusion coefficient D (m^2 s^{-1}).

$$\omega_D = D/d_{eff}^2 \quad (15)$$

The diffusion impedance, expressed by eqn (16), where R_d is the diffusion resistance (Ω m^2), assumes a Nernst stagnant

diffusion layer[77] and it is commonly used to fit the low-frequency part of impedance spectra.[185]

$$Z_d = R_d(\tanh(j\omega/\omega_D)^{0.5}/(j\omega/\omega_D)^{0.5}) \quad (16)$$

A diffusion-boundary layer thickness in between 106 and 299 μm was calculated by ter Heijne *et al.*[172] and proved to be in good agreement with previous calculations applying a linear diffusion model for the same system.[186] An increase in ω_D with the flow rate reflected a reduction in the boundary layer thickness, and hence an improved mass transfer of oxygen for the reduction reactions carried out at the biocathode.

The interfacial capacitance was also analyzed by the same authors, for the same interface. This was calculated by using the C_{HM} equation. C_{HM} magnitudes were reported to be around 1 mF cm^{-2},[172] which are about 100 times larger than the specific capacitance associated with an electric surface-charge layer (10 μF cm^{-2}), also called the Helmholtz layer. Such capacitance values were explained to possibly originate from electron accumulation in the cell-surface of the bacteria involved in the biofilm (redox or chemical capacitance) or from proton insertion into the porous cathode material.

The unexpectedly large capacitance values could be an artifact of an inaccurate estimation of the effective capacitance using the C_{HM} equation. Table 1 presents the parameters obtained for the equivalent circuit proposed by ter Heijne *et al.*,[172] including the interfacial capacitance values calculated through the C_{HM} equation. In the same table, the effective capacitances recalculated through the power-law model are presented.

The effective capacitances calculated through both models differ by one order of magnitude: C_{HM} is approximately 1 mF cm^{-2}, while C_{eff} is about 0.1 mF cm^{-2}. The latter is still 10 times higher than what is expected for the Helmholtz layer. Moreover, if the hypothesized equivalent-circuit model and interpretation given by ter Heijne *et al.*[172] are physically-accurate, then the thickness of the film where "electron accumulation" occurs—that is, electrochemically-active biofilm thickness—could be extracted from the capacitance data. In this review, film thickness for both cases is defined by eqn (13). Through both models, the calculated film thickness is significantly smaller than what would be expected for a biofilm. The characteristic thickness of the Helmholtz layer, on the other hand, in aqueous solutions is typically in the scale of a few nanometers and it decreases with increasing the concentration of the electrolyte.[187]

The values of film thickness estimated using the power-law, assuming a constant dielectric permittivity of 80 and the resistivity at the interface of 200 Ω cm (based on the experimental conductivity of the electrolyte), are in the order of nanometer units. A possible explanation for this would be the choice of a fewer parameters than those that would describe a fully-physically-meaningful model. As previously stated by Orazem and Tribollet,[188] "...the objective of a model is not to provide a good fit with the smallest number of parameters. The objective is rather to use the model to gain physical understanding of the system. The model should be able to account for, or at least to be consistent with, all experimental observations".

The equivalent circuit model proposed by ter Heijne *et al.* is[172] presented in Fig. 8a. This electric analogue considers diffusive transport across a boundary layer, which is mainly determined by the hydrodynamic boundary layer, in parallel with a CPE (Q) that associates to the double layer capacitance at the film–solution interface and may also represent charge accumulation in the biofilm or substratum. This model does not explicitly consider the biofilm contribution to the total interface. When considering the EEC represented in Fig. 8b, which additionally includes the biofilm contribution (BF), in parallel to the boundary layer contribution and to the Helmholtz layer (H), different results are obtained.

The calculations for reviewing this aspect considered fixed the parameters obtained by ter Heijne *et al.*,[172] except for the constant phase-element parameters Q and α, especially because the electrolyte resistance is physically explained by the experimental data and Z_d was already validated through previously described methods.[70,172] EIS model parameters (only those differing from those obtained by ter Heijne *et al.*[172]), for the electrical analogue presented in Fig. 8b, are $Q_H = 0.176\ \Omega^{-1}\ s^{\alpha_H}$, $\alpha_H = 0.85$, $Q_{BF} = 65.14 \times 10^{-8}\ \Omega^{-1}\ s^{\alpha_{BF}}$, and $\alpha_{BF} = 0.8469$. In this way, the effective capacitances for both layers are $C_H = 0.9$ mF cm^{-2} and $C_{BF} = 3.16 \times 10^{-6}$ mF cm^{-2}. Film thickness calculated for both dielectrics is $\delta_H = 0.06$ nm and $\delta_{BF} = 19.8$ μm, respectively.

These values would better explain the experimental data. As proven by different investigations and several validated numerical models,[189,190] biofilm thickness in MXC is maximally about 40 μm.[70] Then, the high interfacial capacitance may be not correlated to the biofilm and its presumptive charge-accumulation. Some investigations point out that such high capacitances (in the same order of magnitude as the ones obtained here) can be explained for solid-electrolyte interfaces formed on carbon particles, as a result of their large active surface area, functionalization, and porosity.[191,192] Consequently, it must be pointed out that when referring here to the capacitance values, and in numerous other articles, we only consider the projected surface area of the electrodes in order to achieve practical comparisons with other investigations. For this reason mainly, δ_H may give the impression of being small. However, in the particular case of membrane-electrode assemblies (MEAs) for gas-diffusion electrodes, the concerned surface area also includes the internal porous structure through which the gases diffuse (*i.e.* oxygen through air-cathodes) and a better

Table 1 EIS model parameters. Q and α were obtained for the equivalent circuit proposed by ter Heijne *et al.*, and C_{HM} values were calculated by these authors.[172] C_{eff} stands for the effective capacitances obtained through the power law model (eqn (10)) and δ for the thickness of the dielectric layer associated to the respective capacitances. The value for ρ_δ was considered to be 200 Ω cm, as it is the practical value of the catholyte described in the original article, and biofilm is known to be represented in more than 95% of an aqueous electrolyte

Flow rate [cm s^{-1}]	Q [Ω^{-1} cm$^{\alpha}$]	α	C_{HM} [mF cm^{-2}]	δ_{HM} [nm]	C_{eff} [mF cm^{-2}]	δ_{eff} [nm]
2.8	0.0176	0.851	0.924	0.077	0.093	0.763
2.4	0.0176	0.852	0.922	0.077	0.096	0.742
2.0	0.0175	0.853	0.920	0.077	0.098	0.726
1.7	0.0176	0.850	0.936	0.076	0.092	0.774
1.4	0.0177	0.849	0.946	0.075	0.090	0.789
0.7	0.0179	0.847	0.975	0.073	0.087	0.814
0.000	0.0163	0.873	0.755	0.094	0.137	0.517

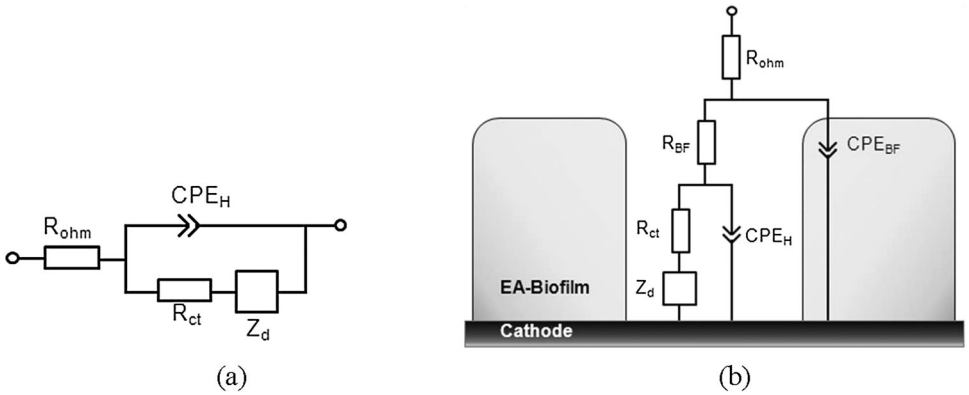

Fig. 8 Equivalent circuits employed to model charge transfer and finite-length diffusion Z_d. (a) EEC proposed by ter Heijne *et al.*,[172] (b) EEC proposed in this article for describing the same system as ter Heijne *et al.* R_{ct} is the charge transfer resistance and CPE_H models the effective capacitance associated to the Helmholtz layer. R_{BF} is the biofilm resistance and CPE_{BF} models the effective capacitance associated to the electrochemically-active (EA) biofilm. R_{ohm} is the electrolyte resistance. The geometrical justification of the system is taken into consideration for a justified interpretation.

visualization of the capacitance values would be derived from the real surface area or mass-based-calculations. Usually, the characteristic thickness of the Helmholtz layer in aqueous solutions is typically in the scale of a few nanometers, but it decreases with increasing concentration of the electrolyte[187] as expected in the case of porous electrodes due to the numerous possible electrostatic interactions, δ_H is indeed expected to appear decreased in comparison to the usual scale in a planar electrode.

Moreover, in the same investigation, by ter Heijne *et al.*,[172] the Sherwood number, which represents the ratio of convective to diffusive mass transport, was determined. They calculated this dimensionless number using eqn (17), where D_T is the hydraulic diameter $2WH/(W + H)$, W the width (2 cm), H the height (1.5 cm), L the channel length (12 cm).

$$\mathrm{Sh} = 3.66(1 + 0.095\mathrm{Pe}D_T/L) \quad (17)$$

Pe is the dimensionless Peclet number, as defined by eqn (18), where ν is the flow velocity and D the diffusion coefficient for oxygen in water.

$$\mathrm{Pe} = D_T\nu/D \quad (18)$$

Tribollet *et al.*[183] showed a graphical method to determine Schmidt numbers from impedance data, for the case of a rotating disk electrode. According to Newman and Thomas-Alyea,[193] this should be applicable to other systems in which transient mass-transfer to an electrode may occur. In the low-frequency range, the effect of the Helmholtz layer and the biofilm layer capacitances may be neglected (*i.e.* when $\omega \to 0$, $Z_{CPE} = 1/j\omega Q \to \infty$), and the total impedance may appear as the sum of $R_{ohm} + R_b + R_{ct} + Z_d$, for an electrochemical system described in Fig. 8b. Given that only Z_d is frequency dependent, when the frequency tends toward zero, the total impedance is dominated by the diffusion limitations. When frequency tends to zero, then Z_d is proportional to the dimensionless function $-1/\theta(0)$, where $-1/\theta(0)$ depends only on the Schmidt number Sc and the dimensionless perturbation frequency represented by eqn (19), with Ω as the rotation speed.

$$p = \omega/\Omega \quad (19)$$

Therefore, the value of Sc is obtained by solving eqn 20 (valid for Sc > 100), where sl is the slope of the straight line $\lambda\mathrm{Sc}^{1/3}$, obtained by plotting ReZ *vs.* pImZ in the low-frequency region.[183]

$$1.2261\mathrm{Sc}^{2/3} + (0.84 - \mathrm{sl})\mathrm{Sc}^{1/3} + 0.63 = 0 \quad (20)$$

For the impedance results from ter Heijne *et al.*,[172] the ReZ *vs.* pImZ plots obtained for the different rotational speeds (calculated in rad s^{-1}) are presented in Fig. 9 for the lowest frequencies measured.

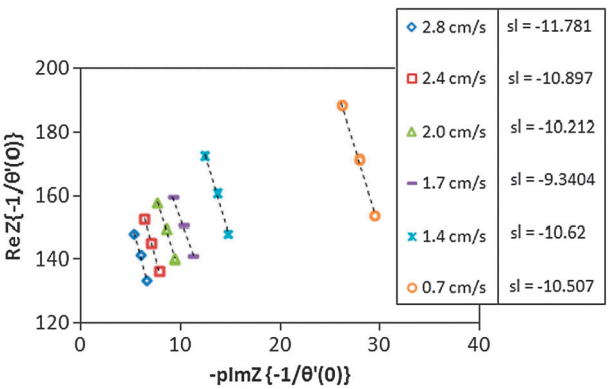

Fig. 9 Variation of the real part of the finite-diffusion-limited impedance *vs.* the imaginary part × the dimensionless frequency. Results are plotted for different flow rates. Slope values (s) for each curve are presented.

Table 2 Dimensionless parameters, Sc and Sh, obtained through the graphical method presented by Tribollet *et al.*[183] Sh results are compared to those obtained by ter Heijne *et al.*, calculated using eqn (17)

Flow rate [cm s^{-1}]	Sc from the graphical method	Sh from Sc obtained by the graphical method	Sh from calculations as stated by ter Heijne *et al.*[172]
2.8	521	167	139
2.4	505	141	130
2.0	517	118	121
1.7	512	96	112
1.4	494	107	101
0.7	525	77	76

Table 3 Equivalent electrical circuits commonly used for representing MXCs single electrode interfaces (anode and cathode) and full cell systems

Modeled case	Circuit proposed	Ref.
Single electrode (e): cathode (c) or anode (a)	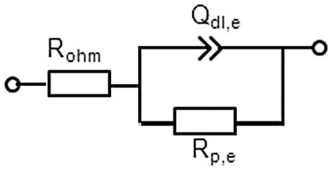	121, 195, 196, 198
	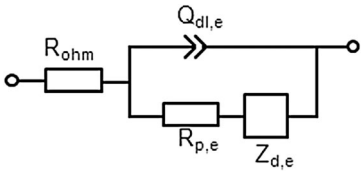	68,130,199
	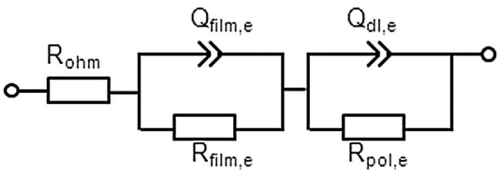	Ref. 115,195,200. Some cases add a diffusional element in series to $R_{film,e}$.[121]
	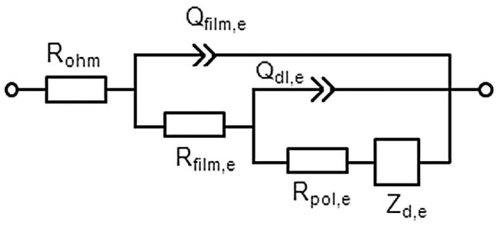	Ref. 67 and this article.
	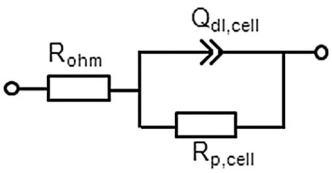	68
	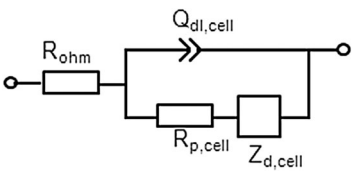	69,89
Full cell	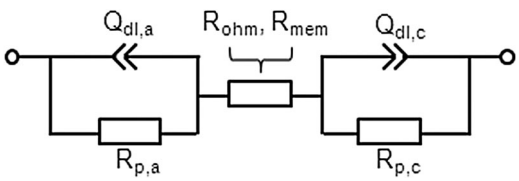	Ref. 140,159,195,197. Some cases add a diffusional element in series to R_p.[71,72,131]
	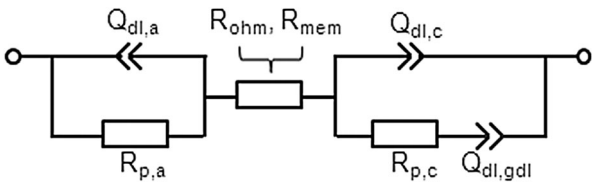	194

Abbreviations: R_{ohm}, ohmic resistance; $Q_{dl,e}$, constant phase element associated to the double layer at the electrode, e; $R_{p,e}$, polarization resistance at the respective electrode; Z_d, Warburg impedance associated to diffusional limitations; $Q_{film,e}$, constant phase element associated to a film developed at the electrode; $R_{film,e}$, resistance at the respective film developed at the electrode; R_{mem}, membrane resistance.

The Sc magnitudes calculated through this method are presented in Table 2. The Sh number can be correlated to Sc, as presented in eqn (21).

$$\mathrm{Sh} = 3.66(1 + 0.095(D_T/L)(D_T\nu\rho\mathrm{Sc}/\mu))^{0.45} \quad (21)$$

When using this method, no significant deviations are observed between Sh obtained using the graphical-method calculations and the equation (based on theoretical values) used by ter Heijne *et al.*,[172] being consistent with the EEC model presented in Fig. 8b.

Finally, it must be noted that the properties of the system (D, ρ, ν, μ) are usually treated as constants, which is not completely valid since they depend on the intrinsic heterogeneity and composition of the (bio)electrochemical interface. On the whole, the use of such constants provides reasonable averaged values.[193] Even so, distribution functions for such properties may be introduced for more comprehensive descriptions in this direction.

3.3 Models with equivalent electric circuits

This review has thus far little encouraged the use of plain EEC for the analysis and interpretation of EIS. The reason for this is because, in practice, most cases use them as a simple means to fit data and obtain a single parameter, *e.g.* R_{ct}, instead of considering the originating hypotheses involving geometrical characteristics, reaction sequences, mass transfer, adsorption and other physical phenomena. Nonetheless, at the end, numerous complex transfer functions derived by solving a well-rationalized process model can be expressed within the mathematical formalism of EEC.[77]

Under such circumstances, taking advantage of this mathematical similarity and simplicity can certainly assist in analyzing the nature of the processes and phenomena occurring in MXCs.

Some common arrangements of electrical analogues are found in the study of MXCs with EIS.[67–69,71–73,89,109,115,119,121,130,140,164,167,168,194–202] Such arrangements are typically not correlated to their geometrical justification, as presented in Fig. 8b, but it is highly advisable to take into account for physical understanding of the current paths.[77]

Three general classes of circuits predominate in EIS analysis applied to MXC: (a) anode, (b) cathode, and (c) full cell; the reported variations of these are described in Table 3. Such schematics cannot be judged as good or bad, simply as poorly justified, as most authors only explain the selection of the electrical elements in terms of generic processes, such as electrical double layers or polarization resistances (which are expected for all practical electrochemical systems)—even if sometimes the experimental data may suggest a contradictory behavior to the proposed model.

The first step to develop equivalent circuit models for electrochemical system is to analyze their overall nature.[77] As obvious as this may appear, it is not systematized for the analysis of EIS data. It is believed here that the major reason for this is that user-friendly dedicated software to fit EIS data is readily available, reducing the necessary efforts needed for physical understanding of the current paths and potential drops in the system, which would certainly be a better guide to structure the corresponding electrical circuit components.

Orazem and Tribollet[77] have carefully explained that when current flowing through circuit elements is the same, but the potential drop is different, the respective impedances must be added in series. Conversely, when current flowing through the circuit elements is different, but the potential drop is the same, the respective impedances must be added in parallel. Using this concept with aid of insightful analysis of the different graphical representations of EIS data provides guidelines for the selection of a suitable circuit.

On the other hand, it should not be forgotten that the nature of the impedance response is not merely electric and the one obtained for the electrochemical systems under study depends on reaction mechanisms and sequences, adsorption, mass transfer and other physical phenomena, sometimes too complex to be reduced to the simplicity of the electrical analogues described here. Improved EIS interpretation will be achieved for MXCs when the frequency response is explained with process or kinetic models, associated to the geometrical distribution of the full-cell or interfacial configuration.

3.4 Mechanistic analysis of the EIS response of MXCs

From this perspective, the opposite circumstance to applying simple equations for EECs occurs: most researchers are discouraged by the mathematical complexity required to develop mechanistic expressions that enable proper analysis of impedance data.[203] Although for some cases the interfacial impedance may be described in terms of simple electrical passive elements, the nature of the impedance response depends on other factors, such as kinetic rates, microbial growth rates, potential and current, mass transfer, surface coverage, hydrodynamics, production of mediators, and all the heterogeneities characteristic of EA-biofilm interfaces, which all in combination affect the mechanisms controlling the electrochemical exchanges within the system. Examples of these models applied to systems other than MXC are provided in the work of Orazem and Tribollet[77] and Macdonald.[203]

Current state of the art on EIS applied to the study of MXCs has not yet provided any of these mechanistic models, but this is expected to become an active challenge of the MXC community towards improvement of the understanding of these systems.

4 Conclusion

The application of electrochemical impedance spectroscopy to the study of microbial electrochemical systems has been proven to improve the fundamental and practical knowledge thereof. Its results have even motivated and supported some major breakthroughs, especially in the MFC technology. Interpretation of EIS data with simple and unjustified electrical analogues will not lead to solid progress in the understanding and improvement of MXCs. The future goal in the use of EIS in the MXC context should be to reveal meaningful mechanisms, processes, limitations and possibilities for improvement. LEIS measurements shall also provide

insight into revealing the distributed-nature of MXC-interfaces. By following the useful guidelines and information provided here, the use, interpretation and evaluation of electrochemical impedance spectroscopy applied to the study of MXCs should be significantly improved and hopefully in the future not anymore unjustifiably employed equivalent electric circuits will be used. As a consequence, the knowledge and evolution of these systems shall be extended to still unexplored areas, especially in the context of the newly-emerging applications, as is the case of microbial electrosynthesis.

Acknowledgements

The authors express their gratitude to Annemiek ter Heijne (Wageningen University, The Netherlands) and Sixto Gimenez (Universitat Jaume I, Spain), for providing their model parameters, here used for the calculations in model-based graphical methods. We are thankful to Abhijeet P. Borole (Oak Ridge National Laboratory), Doug Aaron (Georgia Institute of Technology, USA) and Costas Tsouris (Georgia Institute of Technology and Oak Ridge National Laboratory, USA) for providing the experimental data here used for presenting improved graphical representations. PhD student Blanca Torres-Bautista (CNRS-Université Pierre et Marie Curie, France) is thanked for her contributions to the dimensional analysis of the effective capacitance calculated through the power law model, from CPE parameters. Masters student Ekin Dalak (Université de Toulouse, France) and PhD student Suman Bajracharya (Wageningen University, The Netherlands) are thanked for their contribution to simplify the complicated terminology of this review. The productive and inspiring discussions with Gilbert Van Bogaert (VITO, Belgium) are here appreciated, for their significant contribution to the understanding of fundamental and applied electrochemistry. Last but not least, Xochitl Dominguez-Benetton acknowledges Alain Bergel (CNRS-Université de Toulouse, France) because his contributions to and discussions on the field of microbial electrochemical systems brought a fresh perspective of the field, but especially acknowledges Bernard Tribollet (CNRS-Université Pierre et Marie Curie, France) because his contributions to the improvement of the present article, the exchanges with him in the past years and his influential works on electrochemical impedance spectroscopy were the original motivation for writing this article.

References

1 D. R. Lovley, K. P. Nevin, D. E. Holmes, S. Chauduri, T. Mehta and B. Methe, *Mechanisms for electron transfer to electrodes in mediator-free microbial fuel cells*, 2004.
2 U. Schröder, J. H. Nielsen and F. Scholz, *Angew. Chem., Int. Ed.*, 2003, **42**, 2880.
3 B. H. Kim, I. S. Chang, H. Moon, J. Jang, J. Lee, T. H. Pham and T. N. Phung, *Microbial fuel cells and beyond*, 2004.
4 K. Rabaey and W. Verstraete, *Trends Biotechnol.*, 2005, **23**, 291.
5 B. Logan, *Environ. Sci. Technol.*, 2006, **40**, 5181.
6 D. Pant, G. Van Bogaert, L. Diels and K. Vanbroekhoven, *Bioresour. Technol.*, 2010, **101**, 1533.
7 B. E. Logan, D. Call, S. Cheng, H. V. M. Hamelers, T. H. J. A. Sleutels, A. W. Jeremiasse and R. A. Rozendal, *Environ. Sci. Technol.*, 2008, **42**, 8630.
8 B. Tartakovsky, M. F. Manuel, H. Wang and S. R. Guiot, *Int. J. Hydrogen Energy*, 2009, **34**, 672.
9 L. D. Munoz, B. Erable, L. Etcheverry, J. Riess, R. Bassguy and A. Bergel, *Electrochem. Commun.*, 2010, **12**, 183.
10 A. W. Jeremiasse, H. V. M. Hamelers and C. J. N. Buisman, *Bioelectrochemistry*, 2010, **78**, 39.
11 K. P. Nevin, T. L. Woodard, A. E. Franks, Z. M. Summers and D. R. Lovley, *Ambio*, 2010, **1**, e00103.
12 K. Rabaey and R. A. Rozendal, *Nat. Rev. Microbiol.*, 2010, **8**, 706.
13 K. Rabaey, P. Girguis and L. K. Nielsen, *Curr. Opin. Biotechnol.*, 2011, **22**, 371.
14 K. P. Nevin, S. A. Hensley, A. E. Franks, Z. M. Summers, J. Ou, T. L. Woodard, O. L. Snoeyenbos-West and D. R. Lovley, *Appl. Environ. Microbiol.*, 2011, **77**, 2882.
15 M. Mehanna, P. D. Kiely, D. F. Call and B. E. Logan, *Environ. Sci. Technol.*, 2010, **44**, 9578.
16 X. Cao, X. Huang, P. Liang, K. Xiao, Y. Zhou, X. Zhang and B. E. Logan, *Environ. Sci. Technol.*, 2009, **43**, 7148.
17 H. Luo, P. E. Jenkins and Z. Ren, *Environ. Sci. Technol.*, 2011, **45**, 340.
18 A. T. Heijne, F. Liu, R. v. d. Weijden, J. Weijma, C. J. N. Buisman and H. V. M. Hamelers, *Environ. Sci. Technol.*, 2010, **44**, 4376.
19 M. Rosenbaum, Z. He and L. T. Angenent, *Curr. Opin. Biotechnol.*, 2010, **21**, 259.
20 D. Pant, A. Singh, G. Van Bogaert, S. Irving Olsen, P. Singh Nigam, L. Diels and K. Vanbroekhoven, *RSC Adv.*, 2012, **2**, 1248.
21 K. Rabaey, in *Bioelectrochemical systems: from extracellular electron transfer to biotechnological application*, Nature Publishing Group, a division of Macmillan Publishers Limited, 2009.
22 L. Y. Wang, Y. J. Ye, Y. W. Chen, S. M. Zhu and S. B. Shen, *Xiandai Huagong*, 2010, **30**, 31.
23 H. Liu, R. Ramnarayanan and B. E. Logan, *Environ. Sci. Technol.*, 2004, **38**, 2281.
24 L. T. Angenent, K. Karim, M. H. Al-Dahhan and R. Domiguez-Espinosa, *Trends Biotechnol.*, 2004, **22**, 477.
25 B. Min, J. Kim, S. Oh, J. M. Regan and B. E. Logan, *Water Res.*, 2005, **39**, 4961.
26 H. Gu, X. Zhang, Z. Li and L. Lei, *Chin. Sci. Bull.*, 2007, **52**, 3448.
27 Z. Du, H. Li and T. Gu, *Biotechnol. Adv.*, 2007, **25**, 464.
28 R. A. Rozendal, H. V. M. Hamelers, K. Rabaey, J. Keller and C. J. N. Buisman, *Trends Biotechnol.*, 2008, **26**, 450.
29 N. Lu, S. Zhou, L. Zhuang, J. Zhang and J. Ni, *Biochem. Eng. J.*, 2009, **43**, 246.
30 B. Erable, L. Etcheverry and A. Bergel, *Biofouling*, 2011, **27**, 319.
31 S. T. Oh, J. R. Kim, G. C. Premier, T. H. Lee, C. Kim and W. T. Sloan, *Biotechnol. Adv.*, 2010, **28**, 871.
32 H. M. Poggi-Varaldo, A. Carmona-Martinez, A. L. Vazquez-Larios and O. Solorza-Feria, *J. New Mater. Electrochem. Syst.*, 2009, **12**, 49.
33 A. L. Vazquez-Larios, O. Solorza-Feria, G. Vazquez-Huerta, F. Esparza-Garcia, N. Rinderknecht-Seijas and H. M. Poggi-Varaldo, *Int. J. Hydrogen Energy*, 2011, **36**, 6199.
34 J. M. Foley, R. A. Rozendal, C. K. Hertle, P. A. Lant and K. Rabaey, *Environ. Sci. Technol.*, 2010, **44**, 3629.
35 D. Pant, A. Singh, G. Van Bogaert, Y. A. Gallego, L. Diels and K. Vanbroekhoven, *Renewable Sustainable Energy Rev.*, 2011, **15**, 1305.
36 M. Villano, G. Monaco, F. Aulenta and M. Majone, *J. Power Sources*, 2011, **196**, 9467.
37 M. Villano, *Bioresour. Technol.*, 2010, **101**, 3085.
38 K. Rabaey, K. Van De Sompel, L. Maignien, N. Boon, P. Aelterman, P. Clauwaert, L. De Schamphelaire, H. T. Pham, J. Vermeulen, M. Verhaege, P. Lens and W. Verstraete, *Environ. Sci. Technol.*, 2006, **40**, 5218.
39 E. E. Ferapontova, S. Shleev, T. Ruzgas, L. Stoica, A. Christenson, J. Tkac, A. I. Yaropolov and L. Gorton, in *Perspectives in Bioanalysis Electrochemistry of Nucleic Acids and Proteins: Towards Electrochemical Sensors for Genomics and Proteomics*, ed. F. S. a. Emil Pale-ìek, Elsevier, vol. 1 edn, 2005, pp. 517–598.
40 S. C. Barton, in *Handbook of Fuel Cells*, John Wiley & Sons, Ltd, 2010.
41 J. Zhang, A. M. Kuznetsov, I. G. Medvedev, Q. Chi, T. Albrecht, P. S. Jensen and J. Ulstrup, *Chem. Rev.*, 2008, **108**, 2737.
42 D. R. Lovley, *Environ. Microbiol. Rep.*, 2011, **3**, 27.
43 G. Reguera, R. B. Pollina, J. S. Nicoll and D. R. Lovley, *J. Bacteriol.*, 2007, **189**, 2125.
44 A. Chaubey and B. D. Malhotra, *Biosens. Bioelectron.*, 2002, **17**, 441.
45 R. D. Cusick, B. Bryan, D. S. Parker, M. D. Merrill, M. Mehanna, P. D. Kiely, G. Liu and B. E. Logan, *Appl. Microbiol. Biotechnol.*, 2011, **89**, 2053.

46 S. Sevda and T. R. Sreekrishnan, *J. Environ. Sci. Health, Part A: Toxic/Hazard. Subst. Environ. Eng.*, 2012, **47**, 878.
47 S. Z. Cekic, D. Holtmann, G. Güven, K. M. Mangold, U. Schwaneberg and J. Schrader, *Electrochem. Commun.*, 2010, **12**, 1547.
48 M. Campas i Homs, Universitat Rovira i Virgili, 2003.
49 E. Marsili, *Proc. Natl. Acad. Sci. USA*, 2008, **105**, 3968.
50 K. Rabaey, *ISME J.*, 2007, **1**, 9.
51 S. Parot, M. L. Deülia and A. Bergel, *Electrochim. Acta*, 2008, **53**, 2737.
52 A. P. Borole, G. Reguera, B. Ringeisen, Z. W. Wang, Y. Feng and B. H. Kim, *Energy Environ. Sci.*, 2011, **4**, 4813.
53 S. Parot, M. L. Delia and A. Bergel, *Bioresour. Technol.*, 2008, **99**, 4809.
54 K. Fricke, F. Harnisch and U. Schroder, *Environ. Sci. Technol.*, 2008, **1**, 144.
55 S. M. Strycharz, A. P. Malanoski, R. M. Snider, H. Yi, D. R. Lovley and L. M. Tender, *Energy Environ. Sci.*, 2011, **4**, 896.
56 J. Busalmen, A. Esteve-Nunez, A. Berna and J. M. Feliu, *Angew. Chem., Int. Ed.*, 2008, **47**, 4874.
57 D. R. Lovley, *Curr. Opin. Biotechnol.*, 2008, **19**, 564.
58 R. C. Wagner, D. F. Call and B. E. Logan, *Environ. Sci. Technol.*, 2010, **44**, 6036.
59 H. Richter, K. P. Nevin, H. Jia, D. A. Lowy, D. R. Lovley and L. M. Tender, *Environ. Sci. Technol.*, 2009, **2**, 506.
60 M. Liu, Y. Yuan, L. x. Zhang, L. Zhuang, S. g. Zhou and J. R. Ni, *Bioresour. Technol.*, 2010, **101**, 1807.
61 X. H. Xie, E. L. Li and Z. T. Tang, *Int. J. Environ. Anal. Chem.*, 2010, **5**, 1070.
62 V. J. Watson and B. E. Logan, *Electrochem. Commun.*, 2011, **13**, 54.
63 A. K. Manohar, O. Bretschger, K. H. Nealson and F. Mansfeld, *Electrochim. Acta*, 2008, **53**, 3508.
64 D. Digby, *Electrochim. Acta*, 2006, **51**, 1376.
65 M. E. Orazem, P. Shukla and M. A. Membrino, *Electrochim. Acta*, 2002, **47**, 2027.
66 S. Ouitrakul, M. Sriyudthsak, S. Charojrochkul and T. Kakizono, *Biosens. Bioelectron.*, 2007, **23**, 721.
67 S. Jung, M. M. Mench and J. M. Regan, *Environ. Sci. Technol.*, 2011, **45**, 9069.
68 R. P. Ramasamy, Z. Ren, M. M. Mench and J. M. Regan, *Biotechnol. Bioeng.*, 2008, **101**, 101.
69 M. Rodrigo, P. Canizares, J. Lobato, R. Paz, C. Saez and J. J. Linares, *J. Power Sources*, 2007, **169**, 198.
70 A. ter Heijne, H. V. M. Hamelers, M. Saakes and C. J. N. Buisman, *Electrochim. Acta*, 2008, **53**, 5697.
71 D. Aaron, C. Tsouris, C. Y. Hamilton and A. P. Borole, *Energies (Basel, Switz.)*, 2010, **3**, 592.
72 A. P. Borole, D. Aaron, C. Y. Hamilton and C. Tsouris, *Environ. Sci. Technol.*, 2010, **44**, 2740.
73 Z. He and F. Mansfeld, *Energy Environ. Sci.*, 2009, **2**, 215.
74 D. P. B. T. Strik, A. t. Heijne, H. V. M. Hamelers, M. Saakes and C. J. N. Buisman, *ECS Trans.*, 2008, **13**, 27.
75 J. B. Jorcin, M. E. Orazem, N. Pebere and B. Tribollet, *Electrochim. Acta*, 2006, **51**, 1473.
76 A. K. Manohar, O. Bretschger, K. H. Nealson and F. Mansfeld, *Bioelectrochemistry*, 2008, **72**, 149.
77 M. E. Orazem and B. Tribollet, in *Electrochemical Impedance Spectroscopy*, John Wiley & Sons, Inc., 2008, pp. i–xxxi.
78 P. Agarwal, M. E. Orazem and L. H. Garcia-Rubio, *Electrochim. Acta*, 2005, **41**, 1017.
79 A. J. Bard and L. R. Faulkner, in *Electrochemical methods: fundamentals and applications*, Nature Publishing Group, a division of Macmillan Publishers Limited. All Rights Reserved, 2001.
80 C. Gabrielli, *Identification of Electrochemical Processes by Frequency Response Analysis*, 2011.
81 D. D. Macdonald, John Wiley and Sons Inc., 1991, ch. 11, pp. 515–580.
82 F. Zhao, R. C. T. Slade and J. R. Varcoe, *Chem. Soc. Rev.*, 2009, **38**, 1926.
83 A. Bernard, *Solid State Ionics*, 2004, **169**, 65.
84 M. Urquidi-Macdonald, S. Real and D. D. Macdonald, *Electrochim. Acta*, 1990, **35**, 1559.
85 M. E. Orazem, N. Pebere and B. Tribollet, *J. Electrochem. Soc.*, 2006, **153**, B129.
86 S. Oh, B. Min and B. E. Logan, *Environ. Sci. Technol.*, 2004, **38**, 4900.
87 B. Min, S. Cheng and B. E. Logan, *Water Res.*, 2005, **39**, 1675.
88 Y. Zuo, S. Cheng, D. Call and B. E. Logan, *Environ. Sci. Technol.*, 2007, **41**, 3347.
89 J. R. Kim, G. C. Premier, F. R. Hawkes, R. M. Dinsdale and A. J. Guwy, *J. Power Sources*, 2009, **187**, 393.
90 S. Cheng, H. Liu and B. E. Logan, *Environ. Sci. Technol.*, 2006, **40**, 2426.
91 S. E. Oh and B. E. Logan, *Appl. Microbiol. Biotechnol.*, 2006, **70**, 162.
92 Y. Fan, H. Hu and H. Liu, *Environ. Sci. Technol.*, 2007, **41**, 8154.
93 J. R. Kim, S. Cheng, S. E. Oh and B. E. Logan, *Environ. Sci. Technol.*, 2007, **41**, 1004.
94 B. Logan, S. Cheng, V. Watson and G. Estadt, *Environ. Sci. Technol.*, 2007, **41**, 3341.
95 Y. Zuo, S. Cheng and B. E. Logan, *Environ. Sci. Technol.*, 2008, **42**, 6967.
96 A. Thygesen, F. W. Poulsen, B. Min, I. Angelidaki and A. B. Thomsen, *Bioresour. Technol.*, 2009, **100**, 1186.
97 D. F. Xing, Y. Zuo, S. A. Cheng, J. M. Regan and B. E. Logan, *Environ. Sci. Technol.*, 2008, **42**, 4146.
98 S. You, Q. Zhao, J. Zhang, H. Liu, J. Jiang and S. Zhao, *Biosens. Bioelectron.*, 2008, **23**, 1157.
99 F. Zhao, N. Rahunen, J. R. Varcoe, A. Chandra, C. Avignone-Rossa, A. E. Thumser and R. C. T. Slade, *Environ. Sci. Technol.*, 2008, **42**, 4971.
100 S. Freguia, K. Rabaey, Z. G. Yuan and J. Keller, *Water Res.*, 2008, **42**, 1387.
101 L. Huang and I. Angelidaki, *Biotechnol. Bioeng.*, 2008, **100**, 413.
102 B. Min and I. Angelidaki, *J. Power Sources*, 2008, **180**, 641.
103 D. P. B. T. Strik, H. V. M. Hamelers, J. F. H. Snel and C. J. N. Buisman, *Int. J. Energy Res.*, 2008, **32**, 870.
104 D. Strik, H. Terlouw, H. Hamelers and C. Buisman, *Appl. Microbiol. Biotechnol.*, 2008, **81**, 659.
105 A. Dewan, H. Beyenal and Z. Lewandowski, *Environ. Sci. Technol.*, 2008, **42**, 7643.
106 Y. Fan, E. Sharbrough and H. Liu, *Environ. Sci. Technol.*, 2008, **42**, 8101.
107 M. Di Lorenzo, T. P. Curtis, I. M. Head and K. Scott, *Water Res.*, 2009, **43**, 3145.
108 D. Jiang and B. Li, *Biochem. Eng. J.*, 2009, **47**, 31.
109 Y. Feng, H. Lee, X. Wang, Y. Liu and W. He, *Bioresour. Technol.*, 2010, **101**, 632.
110 J. Y. Nam, H. W. Kim, K. H. Lim, H. S. Shin and B. E. Logan, *Biosens. Bioelectron.*, 2010, **25**, 1155.
111 Y. Sharma and B. Li, *Bioresour. Technol.*, 2010, **101**, 1844.
112 X. Li, B. Hu, S. Suib, Y. Lei and B. Li, *J. Power Sources*, 2010, **195**, 2586.
113 T. Saito, M. D. Merrill, V. J. Watson, B. E. Logan and M. A. Hickner, *Electrochim. Acta*, 2010, **55**, 3398.
114 G. Antonopoulou, K. Stamatelatou, S. Bebelis and G. Lyberatos, *Biochem. Eng. J.*, 2010, **50**, 10.
115 F. Aulenta, *Biosens. Bioelectron.*, 2010, **25**, 1796.
116 M. Di Lorenzo, K. Scott, T. P. Curtis and I. M. Head, *Chem. Eng. J.*, 2010, **156**, 40.
117 H. S. Lee and B. E. Rittmann, *Environ. Sci. Technol.*, 2010, **44**, 948.
118 F. Zhang, D. Pant and B. E. Logan, *Biosens. Bioelectron.*, 2011, **30**, 49.
119 F. Zhang, M. D. Merrill, J. C. Tokash, T. Saito, S. Cheng, M. A. Hickner and B. E. Logan, *J. Power Sources*, 2011, **196**, 1097.
120 Y. Luo, F. Zhang, B. Wei, G. Liu, R. Zhang and B. E. Logan, *J. Power Sources*, 2011, **196**, 9317.
121 R. H. Liu, G. P. Sheng, M. Sun, G. L. Zang, W. W. Li, Z. H. Tong, F. Dong, M. Hon-Wah Lam and H. Q. Yu, *Appl. Microbiol. Biotechnol.*, 2011, **89**, 201.
122 O. Lefebvre, A. Uzabiaga, I. S. Chang, B. H. Kim and H. Y. Ng, *Appl. Microbiol. Biotechnol.*, 2011, **89**, 259.
123 Z. Ren, H. Yan, W. Wang, M. M. Mench and J. M. Regan, *Environ. Sci. Technol.*, 2011, **45**, 2435.
124 V. J. Watson, T. Saito, M. A. Hickner and B. E. Logan, *J. Power Sources*, 2011, **196**, 3009.
125 H. Wang, M. Davidson, Y. Zuo and Z. Ren, *J. Power Sources*, 2011, **196**, 5863.
126 H. Wang, Z. Wu, A. Plaseied, P. Jenkins, L. Simpson, C. Engtrakul and Z. Ren, *J. Power Sources*, 2011, **196**, 7465.
127 X. Xie, L. Hu, M. Pasta, G. F. Wells, D. Kong, C. S. Criddle and Y. Cui, *Nano Lett.*, 2010, **11**, 291.

128 Q. Wen, F. Kong, F. Ma, Y. Ren and Z. Pan, *J. Power Sources*, 2011, **196**, 899.
129 X. Zhang, S. Cheng, P. Liang, X. Huang and B. E. Logan, *Bioresour. Technol.*, 2011, **102**, 372.
130 Y. Zhang, J. Sun, B. Hou and Y. Hu, *J. Power Sources*, 2011, **196**, 7458.
131 Y. Feng, Q. Yang, X. Wang, Y. Liu, H. Lee and N. Ren, *Bioresour. Technol.*, 2011, **102**, 411.
132 S. E. Oh and B. E. Logan, *J. Power Sources*, 2007, **167**, 11.
133 Z. Ren, T. E. Ward and J. M. Regan, *Environ. Sci. Technol.*, 2007, **41**, 4781.
134 Y. Fan, H. Hu and H. Liu, *J. Power Sources*, 2007, **171**, 348.
135 D. Pant, G. Van Bogaert, C. Porto-Carrero, L. Diels and K. Vanbroekhoven, *Water Sci. Technol.*, 2011, **63**, 2457.
136 D. Pant, G. Van Bogaert, M. De Smet, L. Diels and K. Vanbroekhoven, *Electrochim. Acta*, 2010, **55**, 7710.
137 M. D. Merrill and B. E. Logan, *J. Power Sources*, 2009, **191**, 203.
138 A. K. Manohar and F. Mansfeld, *Electrochim. Acta*, 2009, **54**, 1664.
139 Z. He, H. Shao and L. T. Angenent, *Biosens. Bioelectron.*, 2007, **22**, 3252.
140 P. Liang, X. Huang, M. Z. Fan, X. X. Cao and C. Wang, *Appl. Microbiol. Biotechnol.*, 2007, **77**, 551.
141 X. Dominguez-Benetton, Mexican Petroleum Institute, 2007.
142 D. D. Macdonald, Y. A. El-Tantawy, R. C. Rocha-Filho and M. Urquidi-Macdonald, *Evaluation of electrochemical impedance techniques for detecting corrosion on rebar in reinforced concrete*, SHRP-ID/UFR-91-524, SRI International, 1994.
143 R. A. Rozendal, H. V. M. Hamelers, R. J. Molenkamp and C. J. N. Buisman, *Water Res.*, 2007, **41**, 1984.
144 B. E. Logan, B. Hamelers, R. Rozendal, U. Schröder, J. Keller, S. Freguia, P. Aelterman, W. Verstraete and K. Rabaey, *Environ. Sci. Technol.*, 2006, **40**, 5181.
145 Q. Wen, Y. Wu, D. Cao, L. Zhao and Q. Sun, *Bioresour. Technol.*, 2009, **100**, 4171.
146 X. Zhang, S. Cheng, X. Huang and B. E. Logan, *Biosens. Bioelectron.*, 2010, **25**, 1825.
147 K. Rabaey, S. BĂL'tzer, S. Brown, J. Keller and R. A. Rozendal, *Environ. Sci. Technol.*, 2010, **44**, 4315.
148 S. B. Velasquez-Orta, I. M. Head, T. P. Curtis, K. Scott, J. R. Lloyd and H. von Canstein, *Appl. Microbiol. Biotechnol.*, 2010, **85**, 1373.
149 X. Zhang, H. Sun, P. Liang, X. Huang, X. Chen and B. E. Logan, *Biosens. Bioelectron.*, 2011, **30**, 267.
150 S. Cheng, P. Kiely and B. E. Logan, *Bioresour. Technol.*, 2011, **102**, 367.
151 X. Zhang, S. Cheng, X. Wang, X. Huang and B. E. Logan, *Environ. Sci. Technol.*, 2009, **43**, 8456.
152 W. Wang, X. Zhang and J. Wang, *Mater. Corros.*, 2009, **60**, 957.
153 Y. Qiao, C. M. Li, S. J. Bao and Q. L. Bao, *J. Power Sources*, 2007, **170**, 79.
154 X. D. Benetton, S. G. Navarro-Avila and C. Carrera-Figueiras, *J. New Mater. Electrochem. Syst.*, 2010, **13**, 1.
155 Y. Zou, C. Xiang, L. Yang, L. X. Sun, F. Xu and Z. Cao, *Int. J. Hydrogen Energy*, 2008, **33**, 4856.
156 Y. Qiao, S. J. Bao and C. M. Li, *Energy Environ. Sci.*, 2010, **3**, 544.
157 P. Clauwaert, P. Aelterman, T. H. Pham, L. De Schamphelaire, M. Carballa, K. Rabaey and W. Verstraete, *Appl. Microbiol. Biotechnol.*, 2008, **79**, 901.
158 H. S. Lee and B. E. Rittmann, *Int. J. Hydrogen Energy*, 2010, **35**, 920.
159 Z. He, Y. Huang, A. K. Manohar and F. Mansfeld, *Bioelectrochemistry*, 2008, **74**, 78.
160 I. D. Norris, M. M. Shaker, F. K. Ko and A. G. MacDiarmid, *Synth. Met.*, 2000, **114**, 109.
161 J. Niessen, U. Schröder, M. Rosenbaum and F. Scholz, *Electrochem. Commun.*, 2004, **6**, 571.
162 B. Hirschorn, M. E. Orazem, B. Tribollet, V. Vivier, I. Frateur and M. Musiani, *Electrochim. Acta*, 2010, **55**, 6218.
163 B. Hirschorn, M. E. Orazem, B. Tribollet, V. Vivier, I. Frateur and M. Musiani, *J. Electrochem. Soc.*, 2010, **157**, C458.
164 J. N. Zhang, Q. L. Zhao, P. Aelterman, S. J. You and J. Q. Jiang, *Biotechnol. Lett.*, 2008, **30**, 1771.
165 Z. Li, X. Zhang, J. Lin, S. Han and L. Lei, *Bioresour. Technol.*, 2010, **101**, 4440.
166 L. Zhuang, C. Feng, S. Zhou, Y. Li and Y. Wang, *Process Biochem. (Amsterdam, Neth.)*, 2010, **45**, 929.
167 D. W. Liang, S. K. Peng, S. F. Lu, Y. Y. Liu, F. Lan and Y. Xiang, *Bioresour. Technol.*, 2011, **102**, 10881.
168 W. C. Tsan, Y. C. Ming, C. Z. Sheng and T. Shuai, *Int. J. Hydrogen Energy*, 2011, **36**, 9242.
169 C. H. Hsu and F. Mansfeld, *Corrosion (Houston)*, 2001, **57**, 747.
170 P. Cordoba-Torres, T. J. Mesquita, O. Devos, B. Tribollet, V. Roche and R. P. Nogueira, *Electrochim. Acta*, 2012, **72**, 172.
171 G. J. Brug, A. L. G. van den Eeden, M. Sluyters-Rehbach and J. H. Sluyters, *J. Electroanal. Chem. Interfacial Electrochem.*, 1984, **176**, 275.
172 A. ter Heijne, O. Schaetzle, S. Gimenez, F. Fabregat-Santiago, J. Bisquert, D. P. B. T. Strik, F. Barriere, C. J. N. Buisman and H. V. M. Hamelers, *Energy Environ. Sci.*, 2011, **4**, 5035.
173 B. Hirschorn, M. E. Orazem, B. Tribollet, V. Vivier, I. Frateur and M. Musiani, *J. Electrochem. Soc.*, 2010, **157**, C452.
174 N. S. Malvankar, M. Vargas, K. P. Nevin, A. E. Franks, C. Leang, B. C. Kim, K. Inoue, T. Mester, S. F. Covalla, J. P. Johnson, V. M. Rotello, M. T. Tuominen and D. R. Lovley, *Nat. Nanotechnol.*, 2011, **6**, 573.
175 C. Dumas, A. Mollica, D. Feron, R. Basseguy, L. Etcheverry and A. Bergel, *Bioresour. Technol.*, 2008, **99**, 8887.
176 S. R. Taylor, *Prog. Org. Coat.*, 2001, **43**, 141.
177 I. Frateur, V. M. Huang, M. E. Orazem, B. Tribollet and V. Vivier, *J. Electrochem. Soc.*, 2007, **154**, C719.
178 E. Bayet, F. Huet, M. Keddam, K. Ogle and H. Takenouti, *Electrochim. Acta*, 1999, **44**, 4117.
179 V. M. Huang, V. Vivier, I. Frateur, M. E. Orazem and B. Tribollet, *J. Electrochem. Soc.*, 2007, **154**, C89–C98.
180 I. Frateur, *Incentives for using local electrochemical impedance spectroscopy*, 61th Annual Meeting of the International Society of Electrochemistry, 2010.
181 M. Keddam, N. Monfort-Moros and B. Tribollet, *Detection and mapping of SRB influenced corrosion of C-steel*, 2002.
182 R. S. Lillard, P. J. Moran and H. S. Isaacs, *J. Electrochem. Soc.*, 1992, **139**, 1007.
183 B. Tribollet, J. Newman and W. H. Smyrl, *J. Electrochem. Soc.*, 1988, **135**, 134.
184 O. Devos, C. Gabrielli and B. Tribollet, *Electrochim. Acta*, 2006, **51**, 1413.
185 N. Fouquet, C. Doulet, C. Nouillant, G. Dauphin-Tanguy and B. Ould-Bouamama, *J. Power Sources*, 2006, **159**, 905.
186 R. E. Hayes and S. T. Kolaczkowski, *Catal. Today*, 1999, **47**, 295.
187 A. J. Bard and M. Stratmann, in *Encyclopedia of Electrochemistry: Bioelectrochemistry*, Wiley-VCH, 2002.
188 M. E. Orazem and B. Tribollet, *Electrochim. Acta*, 2008, **53**, 7360.
189 C. Picioreanu, I. M. Head, K. P. Katuri, M. C. M. van Loosdrecht and K. Scott, *Water Res.*, 2007, **41**, 2921.
190 C. Picioreanu, M. C. M. van Loosdrecht, T. P. Curtis and K. Scott, *Bioelectrochemistry*, 2010, **78**, 8.
191 K. S. Roy and M. E. Orazem, *J. Electrochem. Soc.*, 2009, **156**, B203.
192 K. Dokko, Y. Fujita, M. Mohamedi, M. Umeda, I. Uchidal and J. R. Selmanl, *Electrochim. Acta*, 2001, **47**, 933.
193 J. S. Newman and K. E. Thomas-Alyea, in *Electrochemical systems*, J. Wiley, 2004.
194 S. You, Q. Zhao, J. Zhang, J. Jiang, C. Wan, M. Du and S. Zhao, *J. Power Sources*, 2007, **173**, 172.
195 Z. He, N. Wagner, S. D. Minteer and L. T. Angenent, *Environ. Sci. Technol.*, 2006, **40**, 5212.
196 S. Srikanth, E. Marsili, M. C. Flickinger and D. R. Bond, *Biotechnol. Bioeng.*, 2008, **99**, 1065.
197 X. Wang, Y. Feng, N. Ren, H. Wang, H. Lee, N. Li and Q. Zhao, *Electrochim. Acta*, 2009, **54**, 1109.
198 P. T. Ha, H. Moon, B. H. Kim, H. Y. Ng and I. S. Chang, *Biosens. Bioelectron.*, 2010, **25**, 1629.
199 M. Sun, F. Zhang, Z. H. Tong, G. P. Sheng, Y. Z. Chen, Y. Zhao, Y. P. Chen, S. Y. Zhou, G. Liu, Y. C. Tian and H. Q. Yu, *Biosens. Bioelectron.*, 2010, **26**, 338.
200 P. Dluglecki, P. Ogonowski, S. J. Metz, M. Saakes, K. Nijmeijer and M. Wessling, *J. Membr. Sci.*, 2010, **349**, 369.
201 D. Aaron, A. P. Borole, S. Yiacoumi and C. Tsouris, *J. Power Sources*, 2012, **201**, 59–65.
202 Y. Zhao, K. Watanabe and K. Hashimoto, *Phys. Chem. Chem. Phys.*, 2011, **13**, 15016.
203 D. D. Macdonald, *Electrochim. Acta*, 1990, **35**, 1509.